Hydrogen and ^{3}He atoms on ^{4}He surfaces: Bound states and scattering features

E. Krotscheck and R. E. Zillich
Institut für Theoretische Physik, Johannes Kepler Universität, A 4040 Linz, Austria
(Received 27 March 2007; published 10 March 2008)

We develop a microscopic theory of atom scattering from inhomogeneous quantum liquids. Methods developed previously for elastic atom scattering and sticking are extended to describe transport currents and inelastic processes. The theory is applied to examine scattering processes of atomic hydrogen and ^{3}He impinging on the surface of liquid ^{4}He at arbitrary angles. For that purpose, we first calculate the ground state of H and ^{3}He on the surface of liquid ^{4}He. We obtain for H a binding energy of about 1 K in good agreement with experiments, and calculate the deformation of the ^{4}He background and impurity-background distribution functions. The angular distribution of the outgoing particle currents generated by inelastic processes is calculated. We pay special attention to the case of small deflection angles as well as to low-energy scattering off third sound modes of the ^{4}He film and off ripplons of the free ^{4}He surface, respectively. In both cases, we obtain an E^2 law for the total direct inelastic scattering probability. Since the self-energy ("optical potential") obtained in our approach is consistent with unitarity, the sticking probability can be calculated using the results for elastic and inelastic scattering. We also investigate the sensitivity of our low-energy results to the long-ranged van der Waals potential of the substrate and to the film thickness.

DOI: 10.1103/PhysRevB.77.094507 PACS number(s): 05.30.Jp, 67.25.dp, 67.25.D−, 67.60.Fp

I. INTRODUCTION

We have developed in recent work[1–3] a manifestly microscopic theory of the dynamics of interactions between single atoms and the surface of liquid ^{4}He. These calculations have provided theoretical tools that are capable of predicting properties such as effective masses, lifetimes, and scattering features of physisorbed impurity atoms. Specializing to ^{3}He impurity atoms, we have highlighted the essential role played by the coupling to surface excitations (ripplons or third sound).

This paper provides, as a natural extension of our previous work, a many-body formulation of inelastic scattering processes from inhomogeneous Bose liquids. A concept that needs to be introduced is that of *second-order* particle currents. These are expectation values of the current operator expanded to second order in the fluctuating part of the many-body scattering wave function which is necessary to describe particle transport. In Ref. 3, we were able to make some statements about inelastic processes using unitarity, but basically at the level of saying "whatever is not elastic must be inelastic." Here, we go much farther. By calculating the aforementioned second-order currents, we can quantitatively obtain the probabilities of scattering into the various inelastic channels. Therefore, our work may be considered as a step toward a completely microscopic formulation of transport phenomena built upon, and consistent with, a quantitative ground-state theory.

We apply these techniques to examine the adsorption and scattering of hydrogen and ^{3}He atoms on the surface of liquid helium films. Atomic hydrogen at low temperatures has yielded interesting physics and applications: spin waves due to the quantum nature of atomic collisions,[4] the cryogenic hydrogen maser,[5] quantum reflection and sticking,[6] as well as three- and two-dimensional quantum gas physics[7] and the possible formation of a quasicondensate.[8,9] The interaction of hydrogen isotopes with the surface of liquid ^{4}He is an important aspect of work with atomic hydrogen[10] and deuterium.[11] Further application of our theoretical tools is envisioned in the theoretical description of evaporative isotopic purification[12] of superfluid ^{4}He.

Particularly important is the fact that the physisorption of H on ^{4}He is remarkably weak. The first semiquantitative estimate[13] of the binding energy of H to the helium surface gave a lower bound of 0.6 K for the binding energy of a H atom on liquid helium, and 2.5 ± 0.6 K for deuterium.[11] Precision measurements of the binding energy of H on liquid helium suggest that the presently best values are from 1.03(2) K (Ref. 14) to 1.14 K (Ref. 15) for H atoms. Earlier work[16,17] reports values of 1.15 ± 0.05 K and 0.89 ± 0.07 K, respectively. The binding energy of D atoms has been found to be 3.97(7) K.[18]

We have already seen that our theoretical description, which was thoroughly tested for the helium liquids, is also valid for hydrogen isotopes in the bulk liquid. There, we have obtained a solvation energy of 14.9 K for D.[19] Extending the calculations of Ref. 19 for atomic H to zero pressure, one obtains a solvation energy of 31.6 K. Of course, the physical scenario studied in this paper is quite different because the impurity atoms cannot easily intrude into the ^{4}He liquid, but we will see that the binding energy of hydrogen to the surface of ^{4}He is also reproduced with good accuracy. The weak adsorption of H atoms allows for some simplification of the theoretical treatment of scattering especially for low energies, which makes the formalism more transparent.

An interesting question related to the interaction of atomic hydrogen with helium films is the problem of quantum reflection.[20,21] One must distinguish between two different aspects of the problem. One is the dependence of scattering and sticking features on the density of states of the hydrogen atom at low energies. The precise nature of the long-ranged van der Waals interaction and, possibly, retardation effects can play important roles. Many-body theory makes no statement on these questions; for a review, see Ref. 22. The sec-

ond question, quite unrelated to the first, is the interaction of the hydrogen atom with the helium surface. Simple estimates can be made based on the knowledge of the surface wave dispersion relation, but the accurate description of how an impinging atom interacts with the helium surface is an intrinsic many-body problem. In that sense, this work is complementary to phenomenological studies of quantum reflection because it provides unambiguous microscopic input to such considerations.

Our paper is organized as follows: In Sec. II, we review the theoretical method of optimizing a correlated N-body wave function to obtain ground-state properties of the background boson liquid and the impurity. Section III explains the method of *time-dependent* correlated wave functions applied to the problem of a single particle scattering at a many-body system, which couples to both virtual and real excitations. The real excitations lead to decay into bound states and scattering channels other than the elastic channel. For calculating transport quantities, the expectation value of the current operator is expanded to second order in the time-dependent correlations. The results are specialized in Sec. IV to the plane surface geometry to obtain probability distributions for direct inelastic scattering. After deriving the basic formulas, we discuss unitarity and inelastic scattering. In Sec. V, we derive low energy–small deflection angle limits for direct inelastic scattering and sticking probabilities for films and free liquid surfaces, and relate these, whenever possible, to other macroscopic observables. Section VI presents an extensive discussion of our results, and Sec. VII gives a brief summary and further prospects.

II. THEORY: STATICS

This paper applies the method of correlated variational wave functions for a microscopic description of scattering phenomena. The implementation of the ground-state theory for the helium surface and atomic impurities, and the treatment of scattering problems have been described in Refs. 1 and 3; we restrict ourselves here to defining the essentials of the theory and give only those equations that are absolutely necessary for the purpose of the discussion of its physical content.

A. Background liquid

The theory begins with the *Jastrow–Feenberg ansatz* for the ground-state wave function of the form

$$\Psi_N(\mathbf{r}_1, \ldots, \mathbf{r}_N) = \exp \frac{1}{2}\left[\sum_i u_1(\mathbf{r}_i) + \sum_{i<j} u_2(\mathbf{r}_i, \mathbf{r}_j) + \sum_{i<j<k} u_3(\mathbf{r}_i, \mathbf{r}_j, \mathbf{r}_k) \right]. \tag{2.1}$$

The only phenomenological input to the theory is the microscopic Hamiltonian

$$H_N = \sum_i \left[-\frac{\hbar^2}{2m_B}\nabla_i^2 + U_{\mathrm{sub}}(\mathbf{r}_i) \right] + \sum_{i<j} V(|\mathbf{r}_i - \mathbf{r}_j|), \tag{2.2}$$

where $V(|\mathbf{r}_i - \mathbf{r}_j|)$ is the ^{4}He-^{4}He interaction, and $U_{\mathrm{sub}}(\mathbf{r})$ is the external "substrate" potential which causes the symmetry breaking.

An essential part of the approach is the *optimization* of the many-body correlations by solving the Euler equations

$$\frac{\delta E_N}{\delta u_n(\mathbf{r}_1, \ldots, \mathbf{r}_n)} = 0 \quad (n = 1,\ 2,\ \text{and}\ 3), \tag{2.3}$$

where E_N is the energy expectation value of the N-particle Hamiltonian (2.2) with respect to the wave function (2.1). The energy is evaluated using the hypernetted chain (HNC) hierarchy of integral equations.[23] The HNC equations provide relationships between the n-body distribution functions

$$g_n(\mathbf{r}_1, \ldots, \mathbf{r}_n) = \frac{\rho_n(\mathbf{r}_1, \ldots, \mathbf{r}_n)}{\rho_1(\mathbf{r}_1) \ldots \rho_1(\mathbf{r}_n)} \tag{2.4}$$

and the correlation functions $u_n(\mathbf{r}_1, \ldots, \mathbf{r}_n)$, where ρ_n are the n-body densities

$$\rho_n(\mathbf{r}_1, \ldots, \mathbf{r}_n) = \frac{N!}{(N-n)!} \frac{\int d^3 r_{n+1} \cdots d^3 r_N \Psi_N^2(\mathbf{r}_1, \ldots, \mathbf{r}_N)}{\int d^3 r_1 \cdots d^3 r_N \Psi_N^2(\mathbf{r}_1, \ldots, \mathbf{r}_N)}. \tag{2.5}$$

These relationships are used to rewrite the ground-state energy in terms of the physical observables $\rho_1(\mathbf{r}_1)$, $g(\mathbf{r}_1, \mathbf{r}_2)$, and $u_3(\mathbf{r}_1, \mathbf{r}_2, \mathbf{r}_3)$,

$$E_N = E_N[\rho_1, g, u_3] = T[\rho_1] + V_{\mathrm{sub}}[\rho_1] + E_c[\rho_1, g, u_3]. \tag{2.6}$$

Here, $T[\rho_1]$ and $V_{\mathrm{sub}}[\rho_1]$ are the kinetic energy of the noninteracting model system and the energy of the particles in the external potential, respectively:

$$T[\rho_1] = \frac{\hbar^2}{2m_B} \int d^3 r |\nabla \sqrt{\rho_1(\mathbf{r})}|^2,$$

$$V_{\mathrm{sub}}[\rho_1] = \int d^3 r \rho_1(\mathbf{r}) U_{\mathrm{sub}}(\mathbf{r}_i). \tag{2.7}$$

$E_c[\rho_1, g, u_3]$ is the "correlation" energy which is a functional of $\rho_1(\mathbf{r}_1)$, $g(\mathbf{r}_1, \mathbf{r}_2)$, and $u_3(\mathbf{r}_1, \mathbf{r}_2, \mathbf{r}_3)$. The ground-state structure of the adsorbed film is now calculated by minimization of the ground-state energy functional (2.6) with respect to the one-body density, the pair-distribution function, and the three-body correlation function for fixed particle number per unit area. Explicit formulas and the essential steps of the algebraic manipulations, as well as the technique used to optimize the triplet correlations, are given in Ref. 24. The resulting one-body equation,

$$\left[-\frac{\hbar^2}{2m_B}\nabla^2 + U_{\text{sub}}(\mathbf{r}) + V_H(\mathbf{r})\right]\sqrt{\rho_1(\mathbf{r})} = \mu_B\sqrt{\rho_1(\mathbf{r})}, \tag{2.8}$$

has the formal structure of a local Schrödinger equation with a self-consistent effective one-body "Hartree potential"

$$V_H(\mathbf{r}) = \frac{\delta E_c}{\delta\rho_1(\mathbf{r})}. \tag{2.9}$$

μ_B is the chemical potential of a background atom.

The two-body equation, resulting from the minimization of the variational energy (2.6) with respect to the pair-distribution function,

$$\frac{\delta E_c}{\delta\sqrt{g(\mathbf{r},\mathbf{r}')}} = 0, \tag{2.10}$$

is best formulated in terms of the (real space) static structure function,

$$S(\mathbf{r},\mathbf{r}') = \delta(\mathbf{r}-\mathbf{r}') + \sqrt{\rho_1(\mathbf{r})\rho_1(\mathbf{r}')}[g(\mathbf{r},\mathbf{r}')-1], \tag{2.11}$$

the one-body Hamiltonian

$$H_1(\mathbf{r}) = -\frac{\hbar^2}{2m_B}\frac{1}{\sqrt{\rho_1(\mathbf{r})}}\nabla\,\rho_1(\mathbf{r})\,\nabla\frac{1}{\sqrt{\rho_1(\mathbf{r})}}, \tag{2.12}$$

and the so-called particle-hole interaction $V_{\text{p-h}}(\mathbf{r},\mathbf{r}')$. The particle-hole interaction is, within the variational theory, defined diagrammatically. It can be represented in terms of the bare interaction and the distribution functions; an explicit form may be found in Ref. 24. In an exact theory, one has also the relationship

$$V_{\text{p-h}}(\mathbf{r},\mathbf{r}') = \frac{\delta V_H(\mathbf{r})}{\delta\rho_1(\mathbf{r}')}. \tag{2.13}$$

A convenient method to solve the Euler equation (2.10) is by normal-mode expansion. We solve the eigenvalue problem

$$\int d^3r'[H_1(\mathbf{r})\delta(\mathbf{r}-\mathbf{r}') + 2\tilde{V}_{\text{p-h}}(\mathbf{r},\mathbf{r}')]H_1(\mathbf{r}')\psi^{(m)}(\mathbf{r}') = \hbar^2\omega_m^2\psi^{(m)}(\mathbf{r}). \tag{2.14}$$

Above, we have introduced the "tilde" notation

$$\tilde{A}(\mathbf{r},\mathbf{r}') \equiv \sqrt{\rho_1(\mathbf{r})}A(\mathbf{r},\mathbf{r}')\sqrt{\rho_1(\mathbf{r}')}. \tag{2.15}$$

The eigenstates $\psi^{(m)}(\mathbf{r})$ of Eq. (2.14) are orthogonal in the metric defined by the one-body operator H_1; a convenient normalization is

$$(\psi^{(m)}|H_1|\psi^{(n)}) = \hbar\omega_m\delta_{m,n}. \tag{2.16}$$

The eigenstates of the adjoint equation

$$\int d^3r' H_1(\mathbf{r})[H_1(\mathbf{r})\delta(\mathbf{r}-\mathbf{r}') + 2\tilde{V}_{\text{p-h}}(\mathbf{r},\mathbf{r}')]\phi^{(m)}(\mathbf{r}') = \hbar^2\omega_m^2\phi^{(m)}(\mathbf{r}) \tag{2.17}$$

are

$$\phi^{(m)}(\mathbf{r}) = \frac{1}{\hbar\omega_m}H_1(\mathbf{r})\psi^{(m)}(\mathbf{r}). \tag{2.18}$$

They can be identified with the density fluctuations in Feynman approximation of the inhomogeneous liquid. The eigenstates satisfy the following orthogonality and completeness relations:

$$(\psi^{(m)}|\phi^{(n)}) = \delta_{m,n},$$

$$\sum_m \psi^{*(m)}(\mathbf{r})\phi^{(m)}(\mathbf{r}') = \delta(\mathbf{r}-\mathbf{r}'). \tag{2.19}$$

The static structure function (2.11) and its inverse, the "direct correlation function" $X(\mathbf{r},\mathbf{r}')$, are obtained from the eigenstates by a normal-mode expansion

$$S(\mathbf{r},\mathbf{r}') = \sum_m \phi^{*(m)}(\mathbf{r})\phi^{(m)}(\mathbf{r}'), \tag{2.20}$$

$$\delta(\mathbf{r},\mathbf{r}') - \tilde{X}(\mathbf{r},\mathbf{r}') = \sum_m \psi^{*(m)}(\mathbf{r})\psi^{(m)}(\mathbf{r}'). \tag{2.21}$$

By construction, the states $\psi^{(m)}(\mathbf{r})$ satisfy the generalized eigenvalue problem

$$H_1(\mathbf{r})\psi^{(m)}(\mathbf{r}) = \hbar\omega_m\int d^3r' S(\mathbf{r},\mathbf{r}')\psi^{(m)}(\mathbf{r}'), \tag{2.22}$$

which is readily identified with the inhomogeneous generalization[25] of the well-known Feynman dispersion relation $\hbar\omega(k)=\hbar^2k^2/[2m_BS(k)]$. These states and their associated energies will be useful quantities for the description of the features of the impurity problem.

B. Impurity atom

Using a simple microscopic model of liquid ^{4}He as a continuum with sharp interface, Zimmerman and Berlinsky[26] showed that for a H atom physisorbed on liquid helium, the coupling to ripplons is just due to the dependence of the binding energy on the curvature of the helium surface. It is difficult to construct such simple paradigms in a truly microscopic theory of the surface because the curvature of the surface is a result of the calculation and not an adjustable input to the description. Nevertheless, our formulation shows, in its essential steps connected with the optimization of the pair correlations, how virtual excitations play an important role.

We adopt the convention that coordinate $\mathbf{r}_0$ refers to the impurity particle and coordinates $\mathbf{r}_i$, with $i=1,\ldots,N$, to the background particles. The Hamiltonian of the $N+1$ particle system consisting of N ^{4}He atoms and one impurity of mass m_I is

$$H^I_{N+1} = -\frac{\hbar^2}{2m_I}\nabla_0^2 + U^I_{\text{sub}}(\mathbf{r}_0) + \sum_{i=1}^N V^I(|\mathbf{r}_0-\mathbf{r}_i|) + H_N, \tag{2.23}$$

where $U^I_{\text{sub}}(\mathbf{r}_0)$ is the impurity-substrate potential, and $V^I(|\mathbf{r}_0-\mathbf{r}_i|)$ is the impurity-^{4}He interaction potential.

The variational wave function (2.1) for an inhomogeneous N-particle Bose system with a single impurity atom is

$$\Psi^I_{N+1}(\mathbf{r}_0,\mathbf{r}_1,\ldots,\mathbf{r}_N) = \exp\frac{1}{2}\Bigg[u^I_1(\mathbf{r}_0) + \sum_{1\le i\le N} u^I_2(\mathbf{r}_0,\mathbf{r}_i) + \sum_{1\le i<j\le N} u^I_3(\mathbf{r}_0,\mathbf{r}_i,\mathbf{r}_j)\Bigg]\Psi_N(\mathbf{r}_1,\ldots,\mathbf{r}_N). \tag{2.24}$$

The impurity chemical potential is $\mu_I \equiv E^I_{N+1} - E_N$, where E^I_{N+1} is the energy of the system containing one impurity and N background atoms, and E_N is the energy (2.6) of the unperturbed background system.

The impurity chemical potential μ_I has a structure similar to that of the background energy,

$$\mu_I = T^I + V^I_{\rm sub} + E_c[\rho^I_1,\rho_1,g^I,g,u^I_3,u_3], \tag{2.25}$$

where

$$T^I = \frac{\hbar^2}{2m_I}\int d^3r_0 |\nabla\sqrt{\rho^I_1(\mathbf{r}_0)}|^2, \quad V^I_{\rm sub} = \int d^3r_0 U^I_{\rm sub}(\mathbf{r}_0)\rho^I_1(\mathbf{r}_0) \tag{2.26}$$

depend only on the impurity density $\rho^I_1(\mathbf{r}_0)$, and the correlation energy part is $E_c[\rho^I_1,\rho_1,g^I,g,u^I_3,u_3]$.

The definitions of the impurity densities

$$\rho^I_n(\mathbf{r}_0,\mathbf{r}_1,\ldots,\mathbf{r}_{n-1}) = \frac{N!}{(N-n+1)!}\frac{\int d^3r_n\cdots d^3r_N|\Psi^I_{N+1}(\mathbf{r}_0,\mathbf{r}_1,\ldots,\mathbf{r}_N)|^2}{\int d^3r_0 d^3r_1\cdots d^3r_N|\Psi^I_{N+1}(\mathbf{r}_0,\mathbf{r}_1,\ldots,\mathbf{r}_N)|^2} \tag{2.27}$$

and the impurity distribution functions

$$g^I_n(\mathbf{r}_0,\mathbf{r}_1,\ldots,\mathbf{r}_{n-1}) = \frac{\rho^I_n(\mathbf{r}_0,\mathbf{r}_1,\ldots,\mathbf{r}_{n-1})}{\rho^I_1(\mathbf{r}_0)\rho_1(\mathbf{r}_1)\cdots\rho_1(\mathbf{r}_{n-1})} \tag{2.28}$$

are used to derive the explicit expression for the impurity correlation energy. One must take into account that all background quantities are changed by the presence of the impurity by terms of the order of $1/N$; these changes give rise to quantitatively important background rearrangement effects. The details of the derivation are given in Refs. 1 and 27.

The impurity density is calculated by minimizing the chemical potential (2.25) with respect to $\sqrt{\rho^I_1(\mathbf{r}_0)}$. This leads again to an effective one-body Schrödinger equation

$$\left[-\frac{\hbar^2}{2m_I}\nabla^2_0 + U^I_{\rm sub}(\mathbf{r}_0) + V^I_H(\mathbf{r}_0)\right]\sqrt{\rho^I_1(\mathbf{r}_0)} = \mu_I\sqrt{\rho^I_1(\mathbf{r}_0)}. \tag{2.29}$$

The operator

$$H^I_1(\mathbf{r}_0) = -\frac{\hbar^2}{2m_I}\frac{1}{\sqrt{\rho^I_1(\mathbf{r}_0)}}\nabla_0\rho^I_1(\mathbf{r}_0)\nabla_0\frac{1}{\sqrt{\rho^I_1(\mathbf{r}_0)}} = -\frac{\hbar^2}{2m_I}\nabla^2_0 + [U^I_{\rm sub}(\mathbf{r}_0) + V^I_H(\mathbf{r}_0)] - \mu_I \tag{2.30}$$

defines through

$$H^I_1(\mathbf{r}_0)\eta^{(\alpha)}(\mathbf{r}_0) = \varepsilon_\alpha\eta^{(\alpha)}(\mathbf{r}_0) \tag{2.31}$$

the spectrum ε_α and the set of states $\eta^{(\alpha)}(\mathbf{r}_0)$. We will label these *impurity states* with Greek subscripts $\boldsymbol{\alpha},\boldsymbol{\beta},\ldots$, whereas the background phonons $\phi^{(m)}(\mathbf{r})$, $\psi^{(n)}(\mathbf{r})$ defined in Sec. II A are labeled with Latin subscripts.

The two-body Euler equation is derived[24,28] by variation of the impurity chemical potential with respect to $\sqrt{g^I(\mathbf{r}_0,\mathbf{r}_1)}$. It can be formulated in terms of the direct correlation function for the impurity $\tilde{X}^I(\mathbf{r}_0,\mathbf{r}_1)$, which is related to the impurity pair-distribution function through the Ornstein–Zernike relation,

$$\sqrt{\rho^I_1(\mathbf{r}_0)\rho_1(\mathbf{r})}[g^I(\mathbf{r}_0,\mathbf{r}) - 1] \equiv S^I(\mathbf{r}_0,\mathbf{r}) = \int d^3r'\tilde{X}^I(\mathbf{r}_0,\mathbf{r}')S(\mathbf{r}',\mathbf{r}). \tag{2.32}$$

The solution of the Euler equations for the impurity correlations is best formulated in the basis of the impurity states $\eta^{(\alpha)}(\mathbf{r}_0)$ and the Feynman phonon states $\phi^{(m)}(\mathbf{r}_1)$ for the background,

$$(\eta^{(\alpha)}|\tilde{X}^I|\phi^{(m)}) = -2\frac{(\eta^{(\alpha)}|\tilde{V}^I_{\text{p-h}}|\phi^{(m)})}{\varepsilon_\alpha + \hbar\omega_m}. \tag{2.33}$$

The expressions for the impurity *particle-hole interaction* $\tilde{V}^I_{\text{p-h}}(\mathbf{r}_0,\mathbf{r}_1)$ introduced in Eq. (2.33) and the self-consistent one-body Hartree potential $V^I_H(\mathbf{r}_0) \equiv \delta E_c/\delta\rho^I_1(\mathbf{r}_0)$ seen by the single impurity have been derived in Ref. 1. The analytic form of $\tilde{V}^I_{\text{p-h}}(\mathbf{r},\mathbf{r}')$ and of $V^I_H(\mathbf{r})$ are immaterial for the further developments, apart from a special feature (to be discussed below) that is important in the infinite half-space. The analytic form (2.33) of $\tilde{X}^I(\mathbf{r},\mathbf{r}')$ will prove crucial for some low-energy scattering results.

III. THEORY: DYNAMICS

A. Equations of motion for time-dependent correlations

The natural generalization of the variational approach to excited states is to allow for time-dependent correlations $u_n(\mathbf{r}_0,\ldots,\mathbf{r}_n;t)$ in the wave function

$$\mathbf{\Phi}(t) = \frac{1}{\sqrt{\langle\psi^I|\psi^I\rangle}}e^{-iE^I_{N+1}t/\hbar}\psi^I(\mathbf{r}_0,\mathbf{r}_1,\ldots,\mathbf{r}_N;t), \tag{3.1}$$

where $\psi^I(\mathbf{r}_0,\mathbf{r}_1,\ldots,\mathbf{r}_N;t)$ contains the time-dependent correlations, again written in a Jastrow–Feenberg form,

$$\psi^I(\mathbf{r}_0,\mathbf{r}_1,\ldots,\mathbf{r}_N;t) = \exp\left[\frac{1}{2}\delta U(\mathbf{r}_0,\mathbf{r}_1,\ldots,\mathbf{r}_N;t)\right]\Psi^I_{N+1}(\mathbf{r}_0,\mathbf{r}_1,\ldots,\mathbf{r}_N), \tag{3.2}$$

$$\delta U(\mathbf{r}_0,\mathbf{r}_1,\ldots,\mathbf{r}_N;t) = \delta u_1(\mathbf{r}_0;t) + \sum_{1\le i\le N} \delta u_2(\mathbf{r}_0,\mathbf{r}_i;t), \tag{3.3}$$

where we neglect fluctuations of correlations between three and more particles. The time-dependent parts $\delta U(\mathbf{r}_0,\mathbf{r}_1,\ldots,\mathbf{r}_N;t)$ of the correlations are determined by the stationary principle

$$\delta\mathcal{S} = \delta\int_{t_0}^{t_1} \mathcal{L}(t)dt = \delta\int_{t_0}^{t_1} \langle\mathbf{\Phi}(t)|H^I_{N+1} - i\hbar\frac{\partial}{\partial t}|\mathbf{\Phi}(t)\rangle dt = 0. \tag{3.4}$$

The variation of the action integral with respect to $\delta u_1^*(\mathbf{r}_0;t)$ and $\delta u_2^*(\mathbf{r}_0,\mathbf{r}_1;t)$ leads to coupled one- and two-particle continuity equations for the *first-order* density fluctuations

$$\delta\rho_1^{(1)}(\mathbf{r}_0;t) \equiv \frac{1}{2}\frac{\langle\Psi^I_{N+1}|\delta U^*\hat\rho^I(\mathbf{r}_0) + \hat\rho^I(\mathbf{r}_0)\delta U|\Psi^I_{N+1}\rangle}{\langle\Psi^I_{N+1}|\Psi^I_{N+1}\rangle} - \rho_1^I(\mathbf{r}_0)\frac{1}{2}\frac{\langle\Psi^I_{N+1}|\delta U + \delta U^*|\Psi^I_{N+1}\rangle}{\langle\Psi^I_{N+1}|\Psi^I_{N+1}\rangle},$$

$$\delta\rho_2^{(1)}(\mathbf{r}_0,\mathbf{r}_1;t) \equiv \frac{1}{2}\frac{\langle\Psi^I_{N+1}|\delta U^*\hat\rho^I(\mathbf{r}_0)\hat\rho(\mathbf{r}_1) + \hat\rho^I(\mathbf{r}_0)\hat\rho(\mathbf{r}_1)\delta U|\Psi^I_{N+1}\rangle}{\langle\Psi^I_{N+1}|\Psi^I_{N+1}\rangle} - \rho_2^I(\mathbf{r}_0,\mathbf{r}_1)\frac{1}{2}\frac{\langle\Psi^I_{N+1}|\delta U + \delta U^*|\Psi^I_{N+1}\rangle}{\langle\Psi^I_{N+1}|\Psi^I_{N+1}\rangle}, \tag{3.5}$$

and currents

$$\mathbf{j}_1^{(1)}(\mathbf{r}_0;t) \equiv \frac{1}{2}\frac{\langle\Psi^I_{N+1}|\delta U^*\hat{\mathbf{j}}^I(\mathbf{r}_0) + \hat{\mathbf{j}}^I(\mathbf{r}_0)\delta U|\Psi^I_{N+1}\rangle}{\langle\Psi^I_{N+1}|\Psi^I_{N+1}\rangle},$$

$$\mathbf{j}_2^{(1)}(\mathbf{r}_0,\mathbf{r}_1;t) \equiv \frac{1}{2}\frac{\langle\Psi^I_{N+1}|\delta U^*\hat{\mathbf{j}}^I(\mathbf{r}_0)\hat\rho(\mathbf{r}_1) + \hat{\mathbf{j}}^I(\mathbf{r}_0)\hat\rho(\mathbf{r}_1)\delta U|\Psi^I_{N+1}\rangle}{\langle\Psi^I_{N+1}|\Psi^I_{N+1}\rangle},$$

$$\mathbf{J}_2^{(1)}(\mathbf{r}_0,\mathbf{r}_1;t) \equiv \frac{1}{2}\frac{\langle\Psi^I_{N+1}|\delta U^*\hat\rho^I(\mathbf{r}_0)\hat{\mathbf{j}}(\mathbf{r}_1) + \hat\rho^I(\mathbf{r}_0)\hat{\mathbf{j}}(\mathbf{r}_1)\delta U|\Psi^I_{N+1}\rangle}{\langle\Psi^I_{N+1}|\Psi^I_{N+1}\rangle}, \tag{3.6}$$

where $\hat\rho^I(\mathbf{r}_0)$, $\hat\rho(\mathbf{r})$, $\hat{\mathbf{j}}^I(\mathbf{r}_0)$, and $\hat{\mathbf{j}}(\mathbf{r})$ are the impurity and background density and current operators. For the specific choice (3.3) of the excitation operator, the equations of motion (3.4) are equivalent to the continuity equations

$$\nabla_0\cdot\mathbf{j}_1^{(1)}(\mathbf{r}_0;t) + \frac{\partial}{\partial t}\delta\rho_1^{(1)}(\mathbf{r}_0;t) = 0, \tag{3.7}$$

$$\nabla_0\cdot\mathbf{j}_2^{(1)}(\mathbf{r}_0,\mathbf{r}_1;t) + \nabla_1\cdot\mathbf{J}_2^{(1)}(\mathbf{r}_0,\mathbf{r}_1;t) + \frac{\partial}{\partial t}\delta\rho_2^{(1)}(\mathbf{r}_0,\mathbf{r}_1;t) = 0. \tag{3.8}$$

From Eqs. (3.5) and (3.6), we obtain for the fluctuating densities and currents

$$\delta\rho_1^{(1)}(\mathbf{r}_0;t) = \rho_1^I(\mathbf{r}_0)\delta u_1(\mathbf{r}_0;t) + \int d^3r_1\rho_2^I(\mathbf{r}_0,\mathbf{r}_1)\delta u_2(\mathbf{r}_0,\mathbf{r}_1;t) - \rho_1^I(\mathbf{r}_0) \times\left(\int d^3r_0'\rho_1^I(\mathbf{r}'_0)\delta u_1(\mathbf{r}'_0;t) + \int d^3r_0'd^3r_1\rho_2^I(\mathbf{r}'_0,\mathbf{r}_1)\delta u_2(\mathbf{r}'_0,\mathbf{r}_1;t)\right),$$

$$\delta\rho_2^{(1)}(\mathbf{r}_0,\mathbf{r}_1;t) = \rho_2^I(\mathbf{r}_0,\mathbf{r}_1)[\delta u_1(\mathbf{r}_0;t) + \delta u_2(\mathbf{r}_0,\mathbf{r}_1;t)] + \int d^3r_2\rho_3^I(\mathbf{r}_0,\mathbf{r}_1,\mathbf{r}_2)\delta u_2(\mathbf{r}_0,\mathbf{r}_2;t) - \rho_2^I(\mathbf{r}_0,\mathbf{r}_1) \times\left(\int d^3r_0'\rho_1^I(\mathbf{r}'_0)\delta u_1(\mathbf{r}'_0;t) + \int d^3r_0'd^3r_2\rho_2^I(\mathbf{r}'_0,\mathbf{r}_2)\delta u_2(\mathbf{r}'_0,\mathbf{r}_2;t)\right), \tag{3.9}$$

$$\mathbf{j}_1^{(1)}(\mathbf{r}_0;t) = \frac{\hbar}{2m_Ii}\left[\rho_1^I(\mathbf{r}_0)\nabla_0\delta u_1(\mathbf{r}_0;t) + \int d^3r_1\rho_2^I(\mathbf{r}_0,\mathbf{r}_1)\nabla_0\delta u_2(\mathbf{r}_0,\mathbf{r}_1;t)\right],$$

$$\mathbf{j}_2^{(1)}(\mathbf{r}_0,\mathbf{r}_1;t) = \frac{\hbar}{2m_Ii}\left\{\rho_2^I(\mathbf{r}_0,\mathbf{r}_1)[\nabla_0\delta u_1(\mathbf{r}_0;t) + \nabla_0\delta u_2(\mathbf{r}_0,\mathbf{r}_1;t)] + \int d^3r_2\rho_3^I(\mathbf{r}_0,\mathbf{r}_1,\mathbf{r}_2)\nabla_0\delta u_2(\mathbf{r}_0,\mathbf{r}_2;t)\right\},$$

$$\mathbf{J}_2^{(1)}(\mathbf{r}_0,\mathbf{r}_1;t) = \frac{\hbar}{2m_Bi}\rho_2^I(\mathbf{r}_0,\mathbf{r}_1)\nabla_1\delta u_2(\mathbf{r}_0,\mathbf{r}_1;t). \tag{3.10}$$

Note that these quantities are defined as operators acting on the *complex* functions $\delta u_1(\mathbf{r}_0;t)$ and $\delta u_2(\mathbf{r}_0,\mathbf{r}_1;t)$. The physical first-order densities (3.5) and currents (3.6) are obtained by taking the real part of the above quantities.

The next task is to turn Eqs. (3.7) and (3.8) into a set of practical equations that can be dealt with numerically. The simplest nontrivial approximation that contains most of the right physics is the *uniform limit approximation*.[23] It is again convenient to work in the basis defined by the phonon states $\phi^{(m)}(\mathbf{r})$ and the impurity states $\eta^{(\alpha)}(\mathbf{r}_0)$. Without loss of generality, we can assume harmonic time dependence. We expand the time-dependent part of the square root of the single-particle density

$$\delta\sqrt{\rho_1(\mathbf{r}_0;t)} = e^{-i\omega t}\sum_{\boldsymbol{\alpha}} r_{\boldsymbol{\alpha}}\eta^{(\boldsymbol{\alpha})}(\mathbf{r}_0) \equiv e^{-i\omega t}\varphi_\omega(\mathbf{r}_0), \quad (3.11)$$

and can write the equation of motion in the form (the derivation can be found in Ref. 1)

$$\hbar\omega r_{\boldsymbol{\alpha}} = \sum_{\boldsymbol{\beta}} [\delta_{\boldsymbol{\alpha\beta}}\varepsilon_{\boldsymbol{\alpha}} + \Sigma_{\boldsymbol{\alpha\beta}}(\omega)] r_{\boldsymbol{\beta}}, \quad (3.12)$$

where

$$\Sigma_{\boldsymbol{\alpha\beta}}(\omega) = -\sum_{\boldsymbol{\gamma m}} \frac{W^{*(\boldsymbol{\alpha})}_{\boldsymbol{\gamma m}} W^{(\boldsymbol{\beta})}_{\boldsymbol{\gamma m}}}{\hbar\omega_{\boldsymbol{m}} + \varepsilon_{\boldsymbol{\gamma}} - \hbar\omega} \quad (3.13)$$

is the impurity self-energy. The impurity-impurity-phonon vertex function occurring in the self-energy (3.13) is

$$W^{(\boldsymbol{\alpha})}_{\boldsymbol{\gamma m}} = \frac{1}{2}\int d^3r_0 \frac{\eta^{(\boldsymbol{\alpha})}(\mathbf{r}_0)\eta^{*(\boldsymbol{\gamma})}(\mathbf{r}_0)}{\sqrt{\rho_1^I(\mathbf{r}_0)}}[\varepsilon_{\boldsymbol{\gamma}} - \varepsilon_{\boldsymbol{\alpha}} - H_1^I(\mathbf{r}_0)]\tilde{X}_{\boldsymbol{m}}(\mathbf{r}_0) \quad (3.14a)$$

$$= -\frac{\hbar^2}{2m_I}\int d^3r_0 \eta^{*(\boldsymbol{\gamma})}(\mathbf{r}_0)\sqrt{\rho_1^I(\mathbf{r}_0)}\nabla_0 X_{\boldsymbol{m}}(\mathbf{r}_0)\cdot\nabla_0\frac{\eta^{(\boldsymbol{\alpha})}(\mathbf{r}_0)}{\sqrt{\rho_1^I(\mathbf{r}_0)}}, \quad (3.14b)$$

$$X_{\boldsymbol{m}}(\mathbf{r}_0) \equiv \int d^3r_1 X^I(\mathbf{r}_0,\mathbf{r}_1)\sqrt{\rho_1(\mathbf{r}_1)}\phi^{(m)}(\mathbf{r}_1). \quad (3.15)$$

$W^{(\boldsymbol{\alpha})}_{\boldsymbol{\gamma m}}$ describes an impurity atom scattering off a background excitation and is given in terms of quantities obtained in the ground-state calculation.

The structure of the dynamic equations (3.12) and (3.13) is of the expected form of an energy-dependent Hartree equation with a self-energy correction involving the energy loss of the impurity particle by generating the excitations of the background system. Equations (3.12) and (3.13) have a form similar to equations obtained in Green's function perturbation theory. An important feature of Eqs. (3.12) and (3.13) is that $\Sigma_{\boldsymbol{\alpha},\boldsymbol{\beta}=0}(\omega)=\Sigma_{\boldsymbol{\alpha}=0,\boldsymbol{\beta}}(\omega)=0$, i.e., the ground state is not changed by the self-energy, because it is obtained by optimization of the energy expectation value using the HNC equations instead of expanding to second order in the correlations.

For the further developments, it will be useful to think of the matrix elements $W^{(\boldsymbol{\alpha})}_{\boldsymbol{\gamma m}}$ as transition matrix elements between two impurity states which depend parametrically on the phonon quantum numbers $\boldsymbol{m}$, i.e., we write

$$W^{(\boldsymbol{\alpha})}_{\boldsymbol{\gamma m}} = (\eta^{(\boldsymbol{\gamma})}|W_{\boldsymbol{m}}(\mathbf{r}_0)|\eta^{(\boldsymbol{\alpha})}) \quad (3.16)$$

with the operator

$$W_{\boldsymbol{m}}(\mathbf{r}_0) = \frac{1}{2}\left[[H_1, X_{\boldsymbol{m}}](\mathbf{r}_0) - \frac{1}{\sqrt{\rho_1^I(\mathbf{r}_0)}}(H_1\tilde{X}_{\boldsymbol{m}})(\mathbf{r}_0)\right]$$
$$= -\frac{\hbar^2}{2m_I}\sqrt{\rho_1^I(\mathbf{r}_0)}[\nabla_0 X_{\boldsymbol{m}}(\mathbf{r}_0)]\cdot\nabla_0\frac{1}{\sqrt{\rho_1^I(\mathbf{r}_0)}}. \quad (3.17)$$

B. Transport currents

The first-order one-body current $\mathbf{j}_1^{(1)}(\mathbf{r}_0;t)$ does not lead to impurity transport, because, for stationary impurity states, it has the same harmonic time dependence as $\delta u_1(\mathbf{r}_0;t)$ and $\delta\sqrt{\rho_1(\mathbf{r}_0;t)}$. The time average of $\mathbf{j}_1^{(1)}(\mathbf{r}_0;t)$ therefore vanishes. Furthermore, Eq. (3.11) shows that $\mathbf{j}_1^{(1)}(\mathbf{r}_0;t)$ decreases as $\sqrt{\rho_1(\mathbf{r}_0)}$ for $\mathbf{r}_0$ far away from the ^{4}He background, thus yielding no outgoing particle flux.

The flux of impurity atoms is given by the nonfluctuating part of the second-order current

$$\mathbf{j}^{(2)}(\mathbf{r}_0) \equiv \frac{1}{4}\frac{\langle\Psi^I_{N+1}|\delta U^*\hat{\mathbf{j}}^I(\mathbf{r}_0)\delta U|\Psi^I_{N+1}\rangle}{\langle\Psi^I_{N+1}|\Psi^I_{N+1}\rangle} \quad (3.18)$$

for the wave functions (3.2) and (3.3). Terms of order $O((\delta U)^3)$ and higher need not be considered.

The second-order current can be expressed in terms of the first-order currents and densities introduced in Eqs. (3.9) and (3.11), and of pair correlation fluctuations as

$$\mathbf{j}^{(2)}(\mathbf{r}_0;t) = \mathbf{j}^{(2)}_{\mathrm{el}}(\mathbf{r}_0;t) + \mathbf{j}^{(2)}_{\mathrm{inel}}(\mathbf{r}_0;t), \quad (3.19)$$

$$\mathbf{j}^{(2)}_{\mathrm{el}}(\mathbf{r}_0;t) = \mathrm{Re}\left[\frac{1}{2\rho_1^I(\mathbf{r}_0)}\delta\rho_1^{*(1)}(\mathbf{r}_0;t)\mathbf{j}_1^{(1)}(\mathbf{r}_0;t)\right], \quad (3.20)$$

$$\mathbf{j}^{(2)}_{\mathrm{inel}}(\mathbf{r}_0;t) = \mathrm{Re}\left[\frac{\hbar}{4m_I}\rho_1^I(\mathbf{r}_0)\int d^3r_1 d^3r_2 A(\mathbf{r}_0;\mathbf{r}_1,\mathbf{r}_2)\right.$$
$$\left.\times\delta u_2^*(\mathbf{r}_0,\mathbf{r}_1;t)\nabla_0\delta u_2(\mathbf{r}_0;\mathbf{r}_2;t)\rho_1(\mathbf{r}_1)\rho_1(\mathbf{r}_2)\right], \quad (3.21)$$

where

$$A(\mathbf{r}_0;\mathbf{r}_1,\mathbf{r}_2) = g_2^I(\mathbf{r}_0,\mathbf{r}_1)\frac{\delta(\mathbf{r}_1-\mathbf{r}_2)}{\rho_1(\mathbf{r}_1)} + [g_3^I(\mathbf{r}_0;\mathbf{r}_1,\mathbf{r}_2)$$
$$- g_2^I(\mathbf{r}_0,\mathbf{r}_1)g_2^I(\mathbf{r}_0;\mathbf{r}_2)]. \quad (3.22)$$

The second-order current $\mathbf{j}^{(2)}(\mathbf{r}_0;t)$ and the second-order density

$$\rho^{(2)}(\mathbf{r}_0;t) \equiv \frac{1}{4}\frac{\langle\Psi^I_{N+1}|\delta U^*\hat{\rho}^I(\mathbf{r}_0)\delta U|\Psi^I_{N+1}\rangle}{\langle\Psi^I_{N+1}|\Psi^I_{N+1}\rangle} \quad (3.23)$$

satisfy a continuity equation

$$\nabla_0\cdot\mathbf{j}^{(2)}(\mathbf{r}_0;t) + \frac{\partial}{\partial t}\rho^{(2)}(\mathbf{r}_0;t) = 0. \quad (3.24)$$

This is obtained from the first-order one- and two-particle continuity equations (3.7) and (3.8) by taking the real part of

$$\delta u_1^*(\mathbf{r}_0)\times\left[\nabla_0\cdot\mathbf{j}_1^{(1)}(\mathbf{r}_0) + \frac{\partial}{\partial t}\delta\rho_1^{(1)}(\mathbf{r}_0)\right] + \int d^3r_1\,\delta u_2^*(\mathbf{r}_0,\mathbf{r}_1)$$
$$\times\left[\nabla_0\cdot\mathbf{j}_2^{(1)}(\mathbf{r}_0,\mathbf{r}_1) + \nabla_1\mathbf{J}_2^{(1)}(\mathbf{r}_0,\mathbf{r}_1) + \frac{\partial}{\partial t}\delta\rho_2^{(1)}(\mathbf{r}_0,\mathbf{r}_1)\right] = 0.$$

Equation (3.18) describes the second-order *impurity* current. The analogous construction for the ^{4}He current can be

written in a very similar manner, but is not considered in this work; however, we note that the second-order ^{4}He current satisfies a continuity equation only in the asymptotic regime, but not inside the ^{4}He system.

The structure (3.19)–(3.21) of the second-order current shows clearly the important role played by the fluctuating pair correlations $\delta u_2(\mathbf{r}_0,\mathbf{r}_i;t)$. These correlations describe the coupling to the excitations of the ^{4}He background in the wave function $\mathbf{\Phi}(\mathbf{r}_0,\ldots,\mathbf{r}_N;t)$ and have the consequence that our description of scattering processes also includes inelastic processes. In the approximations (3.2) and (3.3), these inelastic components consist of

(1) one outgoing impurity atom, leaving the ^{4}He in an excited state or promoting a ^{4}He atom above the chemical potential; the impurity currents of all these processes sum up to $\mathbf{j}^{(2)}_{\text{inel}}$;

(2) states where the impurity atom is physisorbed, depositing its energy into bound excitations of the ^{4}He system or promoting a ^{4}He atom above the chemical potential; these processes do not contribute to an asymptotic impurity current, but to the sticking probability.

The inelastic component of the impurity current is given by the second term of the exact expression (3.19). Again, the simplest nontrivial approximation for the three-point function $A(\mathbf{r}_0;\mathbf{r}_1,\mathbf{r}_2)$ is the uniform limit approximation, which we have also used for obtaining the equation of motion (3.12),

$$A(\mathbf{r}_0;\mathbf{r}_1,\mathbf{r}_2) \approx \frac{\delta(\mathbf{r}_1-\mathbf{r}_2)}{\rho_1(\mathbf{r}_1)} + g(\mathbf{r}_1,\mathbf{r}_2) - 1. \tag{3.25}$$

In this approximation, we can write $\mathbf{j}^{(2)}_{\text{inel}}(\mathbf{r}_0)$ as

$$\begin{aligned}\mathbf{j}^{(2)}_{\text{inel}}(\mathbf{r}_0) &= \text{Re}\,\frac{\hbar}{4m_I i} \\ &\quad\times \int d^3r_1 d^3r_2 \delta\tilde{u}_2^*(\mathbf{r}_0,\mathbf{r}_1)\nabla_0\delta\tilde{u}_2(\mathbf{r}_0;\mathbf{r}_2)S(\mathbf{r}_1,\mathbf{r}_2) \\ &= \text{Re}\,\frac{\hbar}{4m_I i}\sum_{\boldsymbol{m}} \delta\tilde{u}^*_{\boldsymbol{m}}(\mathbf{r}_0)\nabla_0\delta\tilde{u}_{\boldsymbol{m}}(\mathbf{r}_0),\end{aligned} \tag{3.26}$$

where

$$\delta\tilde{u}_{\boldsymbol{m}}(\mathbf{r}_0) = \sum_{\boldsymbol{\alpha}} \eta^{(\boldsymbol{\alpha})}(\mathbf{r}_0)\delta\tilde{u}_{\boldsymbol{\alpha m}} = \int d^3r\,\delta\tilde{u}_2(\mathbf{r}_0,\mathbf{r})\phi^{(\boldsymbol{m})}(\mathbf{r}), \tag{3.27}$$

and the matrix elements $\delta\tilde{u}_{\boldsymbol{\gamma m}} \equiv (\eta^{(\boldsymbol{\gamma})}|\,\delta\tilde{u}_2\,|\phi^{(\boldsymbol{m})})$ of the time-dependent correlations are given by

$$(\varepsilon_{\boldsymbol{\gamma}} + \hbar\omega_{\boldsymbol{m}} - \hbar\omega)\delta\tilde{u}_{\boldsymbol{\gamma m}} = i\hbar\int d^3r_0 \frac{\eta^{*(\boldsymbol{\gamma})}(\mathbf{r}_0)}{\sqrt{\rho_1^I(\mathbf{r}_0)}}\mathbf{j}^{(1)}(\mathbf{r}_0)\cdot\nabla_0 X_{\boldsymbol{m}}(\mathbf{r}_0) \tag{3.28}$$

[cf. Eq. (G.6) of Ref. 1].

The expression (3.26) for the inelastic second-order current can be interpreted in terms of scattering channels, which will become evident in the application to scattering off films in Sec. IV B. Each quantum number $\boldsymbol{m}$ denotes a "channel wave function" $\delta\tilde{u}_{\boldsymbol{m}}(\mathbf{r}_0)$ into which the impurity atom, initially having energy $\hbar\omega$, can decay if allowed by energy conservation (open channel). The first-order density fluctuation $\varphi_\omega(\mathbf{r}_0)$ [Eq. (3.11)] is called elastic channel wave function and accounts for elastic specular reflection, see Sec. IV A. Both $\delta\tilde{u}_{\boldsymbol{m}}(\mathbf{r}_0)$ and $\varphi_\omega(\mathbf{r}_0)$ have the usual quantum mechanical interpretation of a one-body wave function only in the asymptotic region, i.e., where the ground-state background and impurity densities, shown in Fig. 1, are exponentially small. The second-order impurity current $\mathbf{j}^{(2)}_{\text{inel}}(\mathbf{r}_0)$ is, in principle, observable also in the interaction region, but it is detected in scattering experiments only in the asymptotic region.

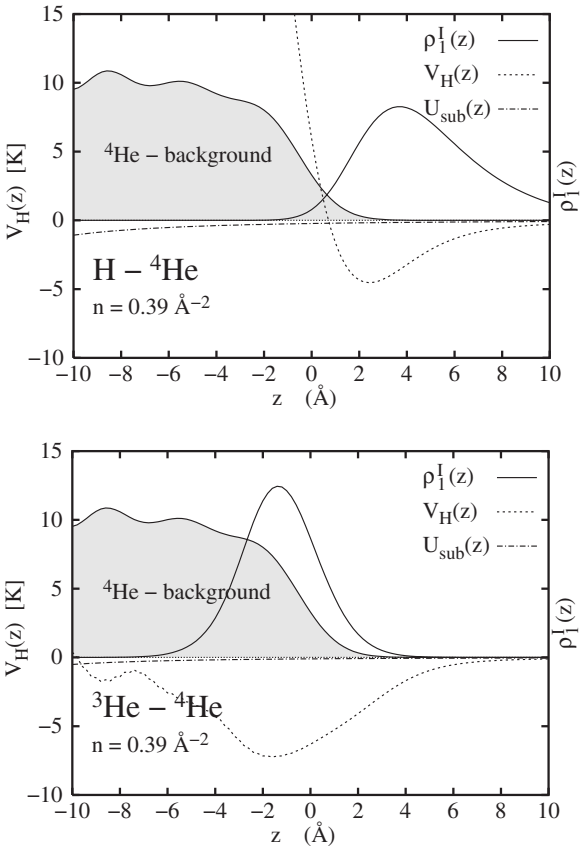

FIG. 1. The figure shows the density profile of the ^{4}He background (shaded region), the ground state $|\Psi(z)|^2$ of the impurity particle, and the effective mean field (Hartree) potential seen by the impurity (dotted line) for H and ^{3}He atoms. The underlying model is always a ^{4}He film with coverage n=0.39 Å^{-2}. Also shown is the bare substrate potential (dash-dotted line).

IV. PLANE SURFACE GEOMETRY

We assume from now on translational invariance in the film plane (x-y plane). Hence, $U_{\text{sub}}(\mathbf{r})$ and $U^I_{\text{sub}}(\mathbf{r}_0)$ are functions of the z coordinate only. Then the ^{4}He density is only a function of the coordinate perpendicular to the film, the z coordinate, $\rho_1(\mathbf{r})=\rho_1(z)$, and the areal density of the film is given by the surface coverage

$$n = \int_0^\infty dz \rho_1(z). \tag{4.1}$$

All states are characterized by two quantum numbers, α and $\mathbf{k}_\alpha$, associated with the motion perpendicular (α) and parallel to the film ($\mathbf{k}_\alpha$). As above, we shall use bold labels (e.g., $\boldsymbol{\alpha}, \boldsymbol{\beta}, \ldots$, for impurity states and $\boldsymbol{m}, \boldsymbol{n}, \ldots$, for film states) to collectively represent both quantum numbers, i.e., $\boldsymbol{\alpha} \equiv \{\alpha, \mathbf{k}_\alpha\}$ and $\boldsymbol{m} \equiv \{m, \mathbf{k}_m\}$.

The phonon states $\phi^{(\boldsymbol{m})}(\mathbf{r})$ and the $X_{\boldsymbol{m}}(\mathbf{r}_0)$ are of the form

$$\phi^{(\boldsymbol{m})}(\mathbf{r}) = \frac{1}{L}\phi^{(m)}(z, \mathbf{k}_m) e^{i\mathbf{k}_m \cdot \mathbf{r}_\parallel}, \quad X_{\boldsymbol{m}}(\mathbf{r}_0) = \frac{1}{L} X_{m,k_m}(z) e^{i\mathbf{k}_m \cdot \mathbf{r}_\parallel}, \tag{4.2}$$

where L^2 is the size of the normalization area in the plane of the film. The energy of state $\phi^{(\boldsymbol{m})}(\mathbf{r})$ is $\hbar\omega_{\boldsymbol{m}} = \hbar\omega_m(k_m)$.

The impurity states $\eta^{(\boldsymbol{\alpha})}(\mathbf{r}_0)$ depend only trivially on the parallel coordinate,

$$\eta^{(\boldsymbol{\alpha})}(\mathbf{r}_0) = \frac{1}{L}\eta^{(\alpha)}(z_0) e^{i\mathbf{k}_\alpha \cdot \mathbf{r}_\parallel}. \tag{4.3}$$

The corresponding energies are

$$\varepsilon_{\boldsymbol{\alpha}} = \epsilon_\alpha(k_\alpha) = \epsilon_\alpha + \frac{\hbar^2 k_\alpha^2}{2m_I}, \tag{4.4}$$

where ϵ_α are the eigenvalues of Eq. (2.31) for $k_\alpha = 0$. In particular,

$$\eta^{(0)}(\mathbf{r}_0) = \frac{1}{L}\sqrt{\rho_1^I(z_0)} e^{i\mathbf{k}_0 \cdot \mathbf{r}_\parallel} \tag{4.5}$$

and $\varepsilon_0 = \hbar^2 k_0^2 / 2m_I$.

The coupling matrix elements (3.14b) depend on the parallel momentum $\mathbf{k}_\alpha$ only through momentum conservation; they have the form

$$(\eta^{(\boldsymbol{\gamma})} | W_{\boldsymbol{m}}(\mathbf{r}_0) | \eta^{(\boldsymbol{\alpha})}) = \frac{1}{L}\delta_{\mathbf{k}_m + \mathbf{k}_\alpha, \mathbf{k}_\gamma} (\eta^{(\gamma)} | W_m(z, \mathbf{k}_m, \mathbf{k}_\alpha) | \eta^{(\alpha)}), \tag{4.6}$$

$$\begin{aligned} W_m(z, \mathbf{k}_m, \mathbf{k}_\alpha) &= \frac{1}{2}\left[[H_1^I(z), X_{m,k_m}(z)] - \frac{1}{\sqrt{\rho_1^I(z)}} [H_1^I(z) \tilde{X}_{m,k_m}(z)] \right. \\ &\quad \left. + \frac{\hbar^2}{m_I} \mathbf{k}_m \cdot \mathbf{k}_\alpha X_{m,k_m}(z) \right] \\ &= -\frac{\hbar^2}{2m_I}\left[\frac{dX_{m,k_m}(z)}{dz} \sqrt{\rho_1^I(z)} \frac{d}{dz} \frac{1}{\sqrt{\rho_1^I(z)}} \right. \\ &\quad \left. - X_{m,k_m}(z) \mathbf{k}_m \cdot \mathbf{k}_\alpha \right]. \end{aligned} \tag{4.7}$$

In coordinate space, and in the adopted plane-surface geometry, Eq. (3.12) reads

$$\left[H_1^I(z) + \frac{\hbar^2 k_\parallel^2}{2m_I} \right] \varphi_\omega(z) + \int dz' \Sigma(z, z', \mathbf{k}_\parallel; \omega) \varphi_\omega(z') = \hbar\omega \varphi_\omega(z), \tag{4.8}$$

where

$$H_1^I(z) = -\frac{\hbar^2}{2m_I} \frac{1}{\sqrt{\rho_1^I(z)}} \frac{d}{dz} \rho_1^I(z) \frac{d}{dz} \frac{1}{\sqrt{\rho_1^I(z)}} \tag{4.9}$$

and

$$\begin{aligned} &\Sigma(z, z', \mathbf{k}_\parallel; \omega) \\ &\quad = -\frac{1}{L^2} \sum_{\gamma, m, \mathbf{k}_m} \frac{W_m^\dagger(z, \mathbf{k}_m, \mathbf{k}_\parallel) \eta^{(\gamma)}(z) \eta^{(\gamma)}(z') W_m(z', \mathbf{k}_m, \mathbf{k}_\parallel)}{\hbar\omega_m(k_m) + \epsilon_\gamma + \dfrac{\hbar^2 (\mathbf{k}_m + \mathbf{k}_\parallel)^2}{2m_I} - \hbar\omega}. \end{aligned} \tag{4.10}$$

Equations (3.12) and (3.13) or, alternatively, Eq. (4.8) determine the energetics of bound states, the impurity motion parallel to the surface, and the dynamics of atom scattering. The solutions have, in configuration space, the form

$$\varphi_\omega(\mathbf{r}) = \varphi_\omega(z) e^{i\mathbf{k}_\parallel \cdot \mathbf{r}_\parallel}. \tag{4.11}$$

Depending on the energy $\hbar\omega$, the solutions describe the motion of physisorbed adatoms ($\hbar\omega < -\mu_I$) or scattering states ($\hbar\omega > -\mu_I$). In the latter case, we can write $\hbar\omega = E - \mu_I = \hbar^2(k_\perp^2 + k_\parallel^2)/2m_I - \mu_I$, where $k_\perp$ and $k_\parallel$ are the perpendicular and parallel components of the wave number for $z \to \infty$, respectively.

A. Elastic scattering and unitarity

The continuum solutions of the effective Schrödinger equation (4.8) describe scattering processes. For a particle impinging with a perpendicular momentum component $k_\perp$ and parallel momentum $\mathbf{k}_\parallel$, $\varphi_\omega(\mathbf{r})$ has the asymptotic form

$$\varphi_\omega(\mathbf{r}) = \varphi_\omega(z) e^{i\mathbf{k}_\parallel \cdot \mathbf{r}_\parallel} \xrightarrow{z \to \infty} e^{i\mathbf{k}_\parallel \cdot \mathbf{r}} [e^{-ik_\perp z} + R(k_\perp, \mathbf{k}_\parallel) e^{ik_\perp z}]. \tag{4.12}$$

Superficially, we appear to be describing a quantum mechanical single-particle scattering problem. In fact, a number of notions such as that of a reflection coefficient can be carried over from single-particle models, but the physical situation is far richer: Since the scattering film is composed of helium atoms, this is a generically *nonlocal* problem when viewed at the one-body level. Moreover, the film is *dynamic*: the incoming particle may produce excited states of the background. This may result in the capture of the particle and/or the emission of particles in states other than the elastic channel. This possibility has been introduced by the inclusion of time-dependent pair correlations and is reflected in the second term of Eq. (3.19), i.e., the expression (3.21).

One of the key quantities of interest is the elastic reflection coefficient $R(k_\perp, \mathbf{k}_\parallel)$. This quantity is directly determined by the coupling of the motion of the impinging particle to the excitations of the quantum liquid. The absolute value of the reflection coefficient can differ from unity only

if the self-energy $\Sigma(\mathbf{r},\mathbf{r}',\omega)$ is non-Hermitian. This happens when the energy denominator in the self-energy (3.13) has zeroes; for scattering solutions, this is the case for all scattering energies $E=\frac{\hbar^2}{2m}(k_\parallel^2+k_\perp^2)$ down to $E\to 0$. A detailed discussion of the elastic reflection coefficient $R(k_\perp,\mathbf{k}_\parallel)$ and its relation to properties of the film as well as results for ^{3}He scattering can be found in Ref. 3.

Unitarity of the *many-body* scattering matrix implies that the sum of all probabilities to scatter into channel $\boldsymbol{m}$ or into the elastic channel is unity. We use this property to obtain the sticking probability s from the asymptotic elastic and inelastic currents, where, for the rest of the paper, the superscript (2) denoting second order is omitted. The elastic current is given by

$$\mathbf{j}_{\mathrm{el}} = -(1-|R|^2)\frac{\hbar k_\perp}{m_I}\mathbf{e}_z + \frac{\hbar}{m_I}\mathbf{k}_\parallel, \tag{4.13}$$

and $\mathbf{j}_{\mathrm{inel}}$ will be calculated in the next section. The integration of the total current $\mathbf{j}=\mathbf{j}_{\mathrm{el}}+\mathbf{j}_{\mathrm{inel}}$ over a plane parallel to and at large distance from the film yields the flux of particles lost due to sticking; the sticking probability is therefore

$$s = 1-|R|^2-\frac{j_{\perp,\mathrm{inel}}}{\hbar k_\perp/m_I} \equiv 1-|R|^2-r_{\mathrm{inel}}, \tag{4.14}$$

where r_{inel} is the probability for inelastic scattering, also called *direct* inelastic scattering as opposed to the combination of sticking and subsequent desorption at finite film temperatures.[29] $|R|^2$ is easily obtained from the equation of motion either by appropriately scaling and fitting the asymptotic form of the solution of Eq. (4.8) to the form (4.12), or by integrating Eq. (4.8) with $\varphi_\omega^*(\mathbf{r})$ and subtracting its complex conjugate:

$$1-|R|^2 = \frac{2m_I}{\hbar^2 k_\perp}\int dz dz' \varphi_\omega^*(z)\,\mathrm{Im}\,\Sigma(z,z',\mathbf{k}_\parallel;\omega)\varphi_\omega(z'), \tag{4.15}$$

where we have again used the asymptotic form (4.12).

We will show in Sec. V B that, for low incident energies $E=\frac{\hbar^2k^2}{2m_I}$, r_{inel} falls off as $r_{\mathrm{inel}}\propto E^2$. Inelastic reflection can, therefore, be neglected compared to $1-|R|^2$ and s for low energies, and we can obtain the sticking coefficient from $s\approx 1-|R|^2$, which is proportional to $\sqrt{E}$ (cf. Refs. 20 and 21; see also Sec. V A). This is no longer valid for energies of the order of 1 K or higher, where all three probabilities $|R|^2$, r_{inel}, and s are of the same order of magnitude.

B. Inelastic scattering

Elastic and inelastic scattering processes are described by their respective asymptotic second-order currents (3.19)–(3.21). According to Eq. (3.26), we can write these currents as

$$\mathbf{j}(z\to\infty) = \mathbf{j}_{\mathrm{el}}+\mathbf{j}_{\mathrm{inel}} = \mathbf{j}_{\mathrm{el}}+{\sum_{\boldsymbol{m}}}'\mathbf{j}_{\mathrm{inel}}^{(\boldsymbol{m})}, \tag{4.16}$$

where the first term is the elastic current (3.20) which takes the asymptotic form (4.13) with wave number $k=(2m_IE)^{1/2}/\hbar$. The second term is the inelastic current which, according to Eq. (3.26), can be written as a sum over the inelastic currents of channel $\boldsymbol{m}$. The prime denotes summation over only *open* inelastic scattering channels, i.e., those where $\delta\tilde{u}_{\boldsymbol{m}}(\mathbf{r}_0)$ is characterized by a real-valued outgoing wave vector.

Having specified the geometry, we will now further evaluate the $\delta\tilde{u}_m(\mathbf{r}_0)$. We assume normalization of all wave functions to a box of length L and $L_\perp$ in the directions parallel and perpendicular to the surface, respectively. According to Eq. (3.28), $\delta\tilde{u}_m(\mathbf{r}_0)$ depends on the first-order current which has the form

$$\mathbf{j}^{(1)}(\mathbf{r}_0) = \mathbf{j}^{(1)}(z_0,\mathbf{k}_\parallel)e^{i\mathbf{k}_\parallel\cdot\mathbf{r}_\parallel}. \tag{4.17}$$

In the uniform limit approximation, we use the Feynman approximation for the incoming current $\mathbf{j}^{(1)}(\mathbf{r}_0)$,

$$\mathbf{j}^{(1)}(\mathbf{r}_0) \approx \frac{\hbar}{2m_I i}\rho_1^I(\mathbf{r}_0)\nabla_0\frac{\delta\rho_1^I(\mathbf{r}_0)}{\rho_1^I(\mathbf{r}_0)} = \frac{\hbar}{m_I i}\rho_1^I(\mathbf{r}_0)\nabla_0\frac{\varphi_\omega(\mathbf{r}_0)}{\sqrt{\rho_1^I(\mathbf{r}_0)}}. \tag{4.18}$$

In this geometry, and with the definitions (3.17) and (4.7), the matrix elements (3.28) of the fluctuating pair correlation induced by the current (4.18) are

$$\begin{aligned}(\varepsilon_\gamma+\hbar\omega_{\boldsymbol{m}}-\hbar\omega)\,\delta\tilde{u}_{\gamma\boldsymbol{m}} &= -2(\eta^{(\gamma)}|W_{\boldsymbol{m}}(\mathbf{r}_0)|\varphi_\omega)\\ &= -\frac{2}{L}\delta_{\mathbf{k}_m+\mathbf{k}_\parallel,\mathbf{k}_\gamma}(\eta^{(\gamma)}|W_m(z,\mathbf{k}_m,\mathbf{k}_\parallel)|\varphi_\omega).\end{aligned} \tag{4.19}$$

We are now ready to calculate

$$\begin{aligned}&\delta\tilde{u}_{\boldsymbol{m}}(\mathbf{r}_0)\\ &= -\frac{2}{L}e^{i(\mathbf{k}_m+\mathbf{k}_\parallel)\cdot\mathbf{r}_\parallel}\sum_\gamma\frac{\eta^{(\gamma)}(z)(\eta^{(\gamma)}|W_m(z',\mathbf{k}_m,\mathbf{k}_\parallel)|\varphi_\omega)}{\epsilon_\gamma+\frac{\hbar^2}{2m_I}(\mathbf{k}_m+\mathbf{k}_\parallel)^2+\hbar\omega_m(k_m)-\hbar\omega}\\ &= \frac{2}{L}e^{i(\mathbf{k}_m+\mathbf{k}_\parallel)\cdot\mathbf{r}_\parallel}\int dz' G(z,z';\epsilon_\lambda)W_m(z',\mathbf{k}_m,\mathbf{k}_\parallel)\varphi_\omega(z'),\end{aligned} \tag{4.20}$$

where $G(z,z';\epsilon_\lambda)$ is the Green's function of the one-body Hamiltonian (4.9) for energy

$$\epsilon_\lambda = \hbar\omega-\frac{\hbar^2}{2m_I}(\mathbf{k}_m+\mathbf{k}_\parallel)^2-\hbar\omega_m(k_m). \tag{4.21}$$

The Green's function may also be written as

$$G(z,z';\epsilon_\lambda) = \frac{2m_I}{\hbar^2}\frac{1}{C}\eta_1^{(\lambda)}(z_>)\eta_2^{*(\lambda)}(z_<), \tag{4.22}$$

where C is the Wronskian of the two linearly independent solutions $\eta_1^{(\lambda)}(z)$ and $\eta_2^{(\lambda)}(z)$ of Eq. (2.29). We are interested in scattering states, i.e., the energy ϵ_λ associated with the state (λ) must be above the evaporation threshold $-\mu_I$ and can, hence, be written as

$$\epsilon_\lambda = -\mu_I + \frac{\hbar^2 k_{\perp,\mathrm{out}}^2}{2m_I}. \tag{4.23}$$

The wave function $\eta_2^{(\lambda)}(z) \equiv \eta^{(\lambda)}(z)$ is regular as $z \to 0$, whereas the irregular solution $\eta_1^{(\lambda)}(z)$ has the form of an outgoing plane wave:

$$\eta_1^{(\lambda)}(z) = \frac{1}{\sqrt{L_\perp}} e^{ik_{\perp,\mathrm{out}} z + i\delta_\lambda}, \quad \eta^{(\lambda)}(z) = \sqrt{\frac{2}{L_\perp}} \sin(k_{\perp,\mathrm{out}} z + \delta_\lambda). \tag{4.24}$$

Then, $C = \sqrt{2} k_{\perp,\mathrm{out}} / L_\perp$, and, hence, for large z,

$$G(z,z';\epsilon_\lambda) \to \frac{2m_I}{\hbar^2 k_{\perp,\mathrm{out}}} e^{ik_{\perp,\mathrm{out}} z + i\delta_\lambda} \eta_\lambda(z'), \quad z \to \infty, \tag{4.25}$$

where we have defined $\eta_\lambda(z) \equiv \sqrt{L_\perp/2}\, \eta^{(\lambda)}(z)$.

We can now go back to Eq. (4.20) and write, for large z,

$$\delta\tilde{u}_{\boldsymbol{m}}(\mathbf{r}_0) = \frac{2m_I}{\hbar^2 k_{\perp,\mathrm{out}}} \frac{2}{L} e^{i[(\mathbf{k}_m + \mathbf{k}_\parallel)\cdot \mathbf{r}_\parallel + k_{\perp,\mathrm{out}} z + \delta_\lambda]} (\eta_\lambda | W_m(z, \mathbf{k}_m, \mathbf{k}_\parallel) | \varphi_\omega)$$

$$\equiv \frac{2}{L} e^{i[(\mathbf{k}_m + \mathbf{k}_\parallel)\cdot \mathbf{r}_\parallel + k_{\perp,\mathrm{out}} z + \delta_\lambda]} M_m(\mathbf{k}_m, \mathbf{k}_\parallel), \tag{4.26}$$

with

$$M_m(\mathbf{k}_m, \mathbf{k}_\parallel) = \frac{2m_I}{\hbar^2 k_{\perp,\mathrm{out}}} (\eta_\lambda | W_m(z, \mathbf{k}_m, \mathbf{k}_\parallel) | \varphi_\omega). \tag{4.27}$$

With this we can now write Eq. (3.26) as

$$\mathbf{j}_{\mathrm{inel}} = {\sum_{m,\mathbf{k}_m}}' \mathbf{j}_{\mathrm{inel}}^{(m,\mathbf{k}_m)} \tag{4.28}$$

with the current of channel $\boldsymbol{m} = (m, \mathbf{k}_m)$ given by

$$\mathbf{j}_{\mathrm{inel}}^{(m,\mathbf{k}_m)} = \frac{\hbar}{m_I L^2} \mathbf{k}_{\mathrm{out}} |M_m(\mathbf{k}_m, \mathbf{k}_\parallel)|^2. \tag{4.29}$$

The wave number of the inelastically scattered impurity is

$$\mathbf{k}_{\mathrm{out}} \equiv \mathbf{k}_m + \mathbf{k}_\parallel + k_{\perp,\mathrm{out}} \mathbf{e}_z,$$

$$k_{\perp,\mathrm{out}}^2 = \frac{2m_I[E - \hbar\omega_m(k_m)]}{\hbar^2} - |\mathbf{k}_{\parallel,\mathrm{out}}|^2. \tag{4.30}$$

It is a function of the energy and the parallel wave number of the incoming current as well as of the energy and wave number of the film mode which is excited. The parallel component $\mathbf{k}_{\parallel,\mathrm{out}}$ is determined by momentum conservation in the direction parallel to the film, whereas the perpendicular component $k_{\perp,\mathrm{out}}$ is determined by energy conservation [Eq. (4.21)]. The prime on the sum in Eq. (4.28) again denotes summation over open channels, where the impurity states are unbound, $\varepsilon_\lambda > |\mu_I|$, i.e., $k_{\perp,\mathrm{out}}$ is real.

From $\mathbf{j}_{\mathrm{inel}}$ we can finally determine r_{inel} as the ratio of the inelastically scattered current perpendicular to the film and the incoming current $\mathbf{j}_{\mathrm{in}} = \hbar\mathbf{k}/m_I$,

$$r_{\mathrm{inel}} = \left| \frac{j_{\perp,\mathrm{inel}}}{j_{\perp,\mathrm{in}}} \right|$$

$$= \frac{2m_I}{\hbar^2 k_\perp} \frac{1}{L^2} {\sum_{m,\mathbf{k}_m}}' \frac{2m_I}{\hbar^2 k_{\perp,\mathrm{out}}} |(\eta_\lambda | W_m(z, \mathbf{k}_m, \mathbf{k}_\parallel) | \varphi_\omega)|^2 \tag{4.31a}$$

$$= \frac{1}{L^2} {\sum_{m,\mathbf{k}_m}}' \frac{k_{\perp,\mathrm{out}}}{k_\perp} |M_m(\mathbf{k}_m, \mathbf{k}_\parallel)|^2. \tag{4.31b}$$

Information about properties of the inelastic currents other than the total probability r_{inel} can be obtained by "binning" into the various decay channels, which amounts to weighing the current operator $\hat{\mathbf{j}}(\mathbf{r})$ with appropriate windowing functions. For example, the expectation value of the operator $\hat{\mathbf{j}}(\mathbf{r}) \delta(\Omega - \Omega_{\hat{\mathbf{j}}})$ gives the differential current, i.e., the current density into the solid angle element $d\Omega$ pointing into the direction $\hat{\mathbf{e}}_\Omega$, where $\Omega_{\hat{\mathbf{j}}}$ is the solid angle in the direction of $\hat{\mathbf{j}}$:

$$\mathbf{j}_{\mathrm{inel}}(\Omega) = {\sum_{\boldsymbol{m}}}' \delta(\Omega - \Omega_{\mathrm{out}}^{(\boldsymbol{m})}) \mathbf{j}_{\mathrm{inel}}^{(\boldsymbol{m})} = \hat{\mathbf{e}}_\Omega {\sum_{\boldsymbol{m}}}' \delta(\Omega - \Omega_{\mathrm{out}}^{(\boldsymbol{m})}) j_{\mathrm{inel}}^{(\boldsymbol{m})}, \tag{4.32}$$

where $\Omega_{\mathrm{out}}^{(\boldsymbol{m})}$ is the solid angle in the direction of the current of channel $\boldsymbol{m}$, $\mathbf{j}_{\mathrm{inel}}^{(\boldsymbol{m})}$, i.e., the direction of $\mathbf{k}_{\mathrm{out}}$. With $\boldsymbol{m} = (m, \mathbf{k}_m)$, the angular current density becomes

$$j_{\mathrm{inel}}(\Omega) = {\sum_m}' \int \frac{d^2 k_m}{(2\pi)^2} \delta(\Omega - \Omega_{\mathrm{out}}^{(m,\mathbf{k}_m)}) j_{\mathrm{inel}}^{(m,\mathbf{k}_m)} \tag{4.33a}$$

$$= \frac{1}{(2\pi)^2} {\sum_m}' {\sum_i} \left[\frac{d\Omega_{\mathrm{out}}^{(m,\mathbf{k}_m)}}{d\mathbf{k}_m} \right]^{-1}_{\mathbf{k}_m^{(i)}} j_{\mathrm{inel}}^{(m,\mathbf{k}_m^{(i)})}, \tag{4.33b}$$

where the $\mathbf{k}_m^{(i)}$ are the (in general, multiple) roots of $\Omega - \Omega_{\mathrm{out}}^{(m,\mathbf{k}_m)} = 0$ and the Jacobian is

$$\left[\frac{d\Omega_{\mathrm{out}}^{(m,\mathbf{k}_m)}}{d\mathbf{k}_m} \right] = \frac{1}{\cos\theta k_{\mathrm{out}}^2} \left| 1 + \hbar \bar{\omega}_m'(k_m) \frac{\mathbf{k}_m \cdot \mathbf{k}_{\parallel,\mathrm{out}}}{k_{\mathrm{out}}^2} \right|. \tag{4.34}$$

$\bar{\omega}_m'(k_m)$ is the derivative of the dispersion relation $\omega_m(k_m)$ with respect to $\frac{\hbar^2 k_m^2}{2m_I}$. We can then define the inelastic differential scattering probability per particle as the ratio between outgoing inelastic current $j_{\mathrm{inel}}(\Omega)$ and incoming current $\frac{\hbar k}{m_I}$,

$$\frac{d\sigma_{\mathrm{inel}}(\Omega)}{d\Omega} = \frac{1}{(2\pi)^2} {\sum_m}' {\sum_i} \left[\frac{d\Omega_{\mathrm{out}}^{(m,\mathbf{k}_m)}}{d\mathbf{k}_m} \right]^{-1}_{\mathbf{k}_m^{(i)}} \frac{k_{\mathrm{out}}}{k} |M_m(\mathbf{k}_m^{(i)}, \mathbf{k}_\parallel)|^2, \tag{4.35}$$

where Eq. (4.29) was used.

Other differential scattering probabilities can be defined in a similar fashion as the ratio between the inelastic current of outgoing energy E_{out} or perpendicular momentum $k_{\perp,\mathrm{out}}$, and the incoming current,

$$\frac{d\boldsymbol{\sigma}_{\mathrm{inel}}(E_{\mathrm{out}})}{dE_{\mathrm{out}}} = \sum_m{}' \int \frac{d^2k_m}{(2\pi)^2}\delta\left(E_{\mathrm{out}} - \frac{\hbar^2 k_{\mathrm{out}}^2}{2m_I}\right) \times \frac{\mathbf{k}_{\mathrm{out}}}{k}|M_m(\mathbf{k}_m,\mathbf{k}_\parallel)|^2, \tag{4.36}$$

$$\frac{d\boldsymbol{\sigma}_{\mathrm{inel}}(\bar{k}_{\perp,\mathrm{out}})}{d\bar{k}_{\perp,\mathrm{out}}} = \sum_m{}' \int \frac{d^2k_m}{(2\pi)^2}\delta(\bar{k}_{\perp,\mathrm{out}} - k_{\perp,\mathrm{out}}) \times \frac{\mathbf{k}_{\mathrm{out}}}{k}|M_m(\mathbf{k}_m,\mathbf{k}_\parallel)|^2. \tag{4.37}$$

The latter would be measured in a time-of-flight experiment, while the first quantity corresponds to measuring the outgoing energy or the energy lost to the film $E-E_{\mathrm{out}}$.

C. Unitarity and relation between s, r_{inel}, and Im Σ

We can now close the circle and relate the result (4.31b) for the inelastic scattering probability r_{inel} to the expression of the elastic reflection probability $|R|^2$, in terms of the imaginary part of the self-energy [Eq. (4.15)].

Taking the limit $L_\perp \to \infty$, the summation over the Hartree states, Σ_γ, in the expression (4.10) for the self-energy consists of a sum over the bound states, Σ_{γ_i}, plus an integral, $\int \frac{dk_{\perp,\gamma}}{\pi}$, over all scattering states of wave number $k_{\perp,\gamma}$ and energy $\epsilon_\gamma = \frac{\hbar^2 k_{\perp,\gamma}^2}{2m_I} - \mu_I$. We define

$$\Sigma_{\gtrless}(z,z',\mathbf{k}_\parallel;\omega) = -\frac{1}{L^2}\sum_{m,\mathbf{k}_m}\sum_\gamma{}^{\gtrless} \frac{W_m^\dagger(z,\mathbf{k}_m,\mathbf{k}_\parallel)\eta^{(\gamma)}(z)\eta^{(\gamma)}(z')W_m(z',\mathbf{k}_m,\mathbf{k}_\parallel)}{\hbar\omega_m(k_m) + \epsilon_\gamma + \frac{\hbar^2(\mathbf{k}_m-\mathbf{k}_\parallel)^2}{2m_I} - \hbar\omega}, \tag{4.38}$$

where the superscripts $>$ and $<$ stand for $\epsilon_\gamma + \mu_I > 0$ and <0, respectively. The imaginary part of $\Sigma_>$ is determined by integration over $k_{\perp,\gamma}$ and using $\frac{1}{x+i\epsilon} = P(\frac{1}{x}) - i\epsilon\delta(x)$:

$$\mathrm{Im}\,\Sigma_>(z,z',\mathbf{k}_\parallel;\omega) = -\frac{2}{L^2}\sum_{m,\mathbf{k}_m}{}' \frac{W_m^\dagger(z,\mathbf{k}_m,\mathbf{k}_\parallel)\eta_\lambda(z)\eta_\lambda(z')W_{\gamma m}(z',\mathbf{k}_m,\mathbf{k}_\parallel)}{\hbar^2 k_{\perp,\mathrm{out}}/m_I}, \tag{4.39}$$

where we have taken the limit $L_\perp \to \infty$. In Eq. (4.39), λ is determined just as for the inelastic current [Eq. (4.21)] and the prime on the sum denotes again summation over open channels, i.e., such that Eq. (4.21) yields $\epsilon_\lambda + \mu_I > 0$, since otherwise Im $\Sigma_>$ vanishes. Comparing with Eq. (4.31b), we find that

$$r_{\mathrm{inel}} = \frac{2m_I}{\hbar^2 k_\perp}\int dz dz' \varphi_\omega^*(z)\mathrm{Im}\,\Sigma_>(z,z',\mathbf{k}_\parallel;\omega)\varphi_\omega(z'). \tag{4.40}$$

By unitarity, the remainder of $1-|R|^2-r_{\mathrm{inel}}$ must be s and the comparison with Eq. (4.15) finally yields

$$s = \frac{2m_I}{\hbar^2 k_\perp}\int dz dz' \varphi_\omega^*(z)\mathrm{Im}\,\Sigma_<(z,z',\mathbf{k}_\parallel;\omega)\varphi_\omega(z'). \tag{4.41}$$

Thus, we conclude that the probability s for the incoming atom to be scattered into any of the sticking channels is given by $2m_I/\hbar^2 k_\perp$ times the expectation value of Im $\Sigma_<$ with respect to the elastic channel wave function φ_ω, where Im $\Sigma_<$ is the contribution of the *bound* Hartree states (i.e., the sticking channels) to Im Σ. Conversely, the probability r_{inel} that the atom is scattered back inelastically is determined by the expectation value of Im $\Sigma_>$, which is the part of Im Σ arising from *scattering* states of the Hartree equation. Intuitively, we expect such a result from an exact calculation, but the fact that our approximate treatment leads to the same conclusion documents the consistency of our treatment because r_{inel} and $1-|R|^2$ were obtained by entirely different calculations.

V. LOW-ENERGY AND SMALL ANGLE SCATTERING

A number of exact statements can be made in the low-energy limit as well as in the limit of the small deflection angles, which both imply low-energy transfer. In particular, we will be able to express some of the *microscopically defined* quantities by macroscopic derivatives, thereby eliminating several diagrammatic approximations. We restrict ourselves for simplicity to scattering perpendicular to the surface, i.e., the parallel momentum $\mathbf{k}_\parallel$ of the incoming current is zero. This poses no restriction for the sticking coefficient $s(\mathbf{k})$ because $s(\mathbf{k})$ depends, in the low-energy limit, only on the perpendicular component of the wave number $k_\perp$, i.e., $s(\mathbf{k}) \to s(k_\perp)$.

A. Low-energy limit of s

The calculation of *low-energy* sticking becomes particularly simple if the impurity attached to the ^{4}He surface has only one bound state. For sufficiently thick films, this is the case for atomic hydrogen which is of interest not only in connection with the observation of universal quantum sticking,[6,30] but also with the possibility of observing a two-

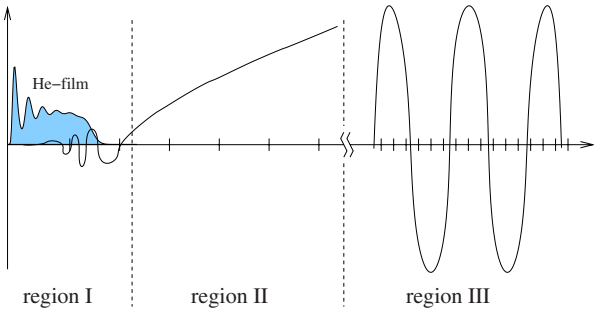

FIG. 2. (Color online) Illustration of the division of the z axis into the three different regions for the discussion of low-energy scattering wave functions in Sec. V A.

dimensional Bose-condensed atomic gas.[8,9,31]

To study the low-energy features of the solutions of either the Hartree equation (2.31) or the full equation of motion (4.8), we divide the z axis into three regions (see Fig. 2): The interaction region I coincides with the actual film region including its surface, i.e., where the film density $\rho_1(z_1)$ is finite; the self-energy is normally complex in this regime. The intermediate region II is where the substrate potential is larger or comparable to the energy of the incoming particle. Finally, the interaction is negligible in the far region III where the atom propagates freely. We give a brief summary of the properties of the solutions of the equation of motion (4.8), and also of the Hartree equation (2.31):

(I) Close to and within the ^{4}He film, only fully solving Eq. (4.8) can yield $\varphi_\omega(z)$. Since E is by assumption much smaller than the interaction energy between the scattered atom and the film, we are allowed to set $E=0$, i.e., $\hbar\omega=|\mu_I|$, in Eq. (4.8). Provided that there is no resonance at $E=0$, the correctly normalized solution can depend, to leading order, only through a scaling factor on the energy. This scaling factor is determined by the *asymptotic* behavior of the solution in region III.

(II) Region II glues regions I and III. We have to distinguish between van der Waals fields that have a potential $U(z)\to -C_3 z^{-3}$, and shorter-ranged substrate potentials (e.g., if retardation is taken into account). The van der Waals potential has been studied in detail in Ref. 32. Equation (4.8) has, for $E=0$, the solution

$$\bar{\varphi}(z) = a\sqrt{z}J_1\left(\sqrt{\frac{D}{z}}\right) + b\sqrt{z}Y_1\left(\sqrt{\frac{D}{z}}\right) \quad \text{with } D = \frac{8m_I C_3}{\hbar^2}, \tag{5.1}$$

where a and b are integration constants. In the limit $C_3=0$, the solution is

$$\bar{\varphi}(z) \sim a_0 + b_0 z. \tag{5.2}$$

(III) The solution in region III is a free wave given by Eq. (4.12)

$$\varphi_\omega(z) = 2i \sin\left[k_\perp\left(z + \frac{\delta_{k_\perp}}{k_\perp}\right)\right]. \tag{5.3}$$

The three expressions for the wave functions in regions I–III match at their respective boundaries. In region I, we can write the wave function of the incoming particle as

$$\varphi_\omega(z) \equiv k_\perp \bar{\varphi}(z), \tag{5.4}$$

where $\bar{\varphi}(z)$ is the zero-energy solution of Eq. (4.8), normalized such that in region II $b=i\pi\sqrt{D}$ or $b_0=2i$, respectively, implying the leading behavior $\bar{\varphi}(z)\sim 2iz$ in region III. The factorization (5.4) of the elastic channel wave function $\varphi_\omega(z)$ in the limit $k_\perp\to 0$ leads for the elastic reflection probability (4.15) to

$$|R(k_\perp)|^2 \to 1 - s_1 k_\perp, \tag{5.5}$$

where the proportionality constant s_1 is determined by the expectation value of $\mathrm{Im}\,\Sigma$ with respect to $\bar{\varphi}(z)$; it will be calculated below. The above low-energy behavior $|R(k_\perp)|^2 \to 1$ is the well-known effect of universal quantum reflection.[20,21]

In the following analysis, we assume that the impinging atom has a single bound (Andreev) state and couples only to the ripplon or third sound modes (i.e., the mode with perpendicular quantum number $m=0$, henceforth denoted by a subscript r). This is the case for H for low scattering energies, but does not apply to ^{3}He which not only has two Andreev states,[33] but also can penetrate into the bulk. A quantitative analysis of the differences between ^{3}He and H scattering will be given in Sec. VI.

We need to retain only the coupling matrix element of the incoming atom to the third sound and the bound state $\eta^{(0)}(z)=\sqrt{\rho_1^I(z)}$,

$$(\eta^{(0)}|W_m(z,\mathbf{k}_m,0)|\bar{\varphi}) = \int dz \bar{\varphi}(z) H_1^I(z) \tilde{X}_{r,k_r}(z), \tag{5.6}$$

which yields for Eq. (4.41)

$$s \to -\frac{2m_I}{\hbar^2 k_\perp}\,\mathrm{Im}\int \frac{d^2k_r}{(2\pi)^2} \frac{|k_\perp(\eta^{(0)}|W_m(z,\mathbf{k}_m,0)|\bar{\varphi})|^2}{\hbar\omega_m(k_m) + \dfrac{\hbar^2 k_m^2}{2m_I} - |\mu_I|}$$

$$\to \frac{m_I k_0 k_\perp}{\hbar^2} \frac{|(\bar{\varphi}|H_1^I(z)|\tilde{X}_{r,k_0})|^2}{\hbar\omega_r'(k_0) + \dfrac{\hbar^2 k_0}{m_I}} \quad \text{for } E\to 0, \tag{5.7}$$

where k_0 is the solution of

$$\hbar\omega_r(k_0) + \frac{\hbar^2 k_0^2}{2m_I} - |\mu_I| = 0. \tag{5.8}$$

In the distorted wave Born approximation (DWBA), $\bar{\varphi}(z)$ in expression (5.7) for s is replaced by the analogously normalized impurity eigenstate $\bar{\eta}(z)$. We can then use the two-body Euler equation (2.33) to write s as

$$s^{\mathrm{DWBA}} \to k_\perp \frac{4m_I k_0}{\hbar^2}\left(\frac{|\mu_I|}{|\mu_I|+\omega_r(k_0)+\frac{\hbar^2 k_0^2}{2m_I}}\right)^2 \frac{|(\bar{\eta}|\tilde{V}_{r,k_0})|^2}{\hbar\omega_r'(k_0)+\frac{\hbar^2 k_0}{m_I}}$$

$$= k_\perp \frac{m_I k_0}{\hbar^2}\frac{|(\bar{\eta}|\tilde{V}_{r,k_0})|^2}{\hbar\omega_r'(k_0)+\frac{\hbar^2 k_0}{m_I}} \quad \text{for } E\to 0, \tag{5.9}$$

where $V_{m,k_m}(z)$ is defined analogously to $X_{m,k_m}(z)$ [see Eq. (3.15)], and Eq. (5.8) was used. A similar result was obtained from a Green's function approach.[34]

The situation is more complicated for scattering of atoms which are bound more strongly to the film, like, for example, ^{3}He. First, falling into a lower chemical potential μ_I releases more energy, and film modes other than the third sound mode, such as bulk and layer phonons and rotons as well as standing waves perpendicular to the surface, can be excited; second, the atom can be trapped into states other than the Andreev state on the surface.[35] Overall, this leads to a larger sticking probability, as we will show in Sec. VI.

B. Low-energy limit of r_{inel} for thin films

We next derive the low-energy limit of r_{inel}. For simplicity, we restrict ourselves again to perpendicular incidence, $\mathbf{k}_\parallel=0$. From the previous section, we know the total inelastic current (4.28). Hence,

$$r_{\mathrm{inel}} = \frac{1}{2\pi}{\sum_m}' \int_0^Q dk_m k_m \frac{k_{\perp,\mathrm{out}}}{k_\perp}|M_m(\mathbf{k}_m,0)|^2, \tag{5.10}$$

where the integration boundary Q assures that $k_{\perp,\mathrm{out}}$ is real; it is determined further below.

We have argued in Sec. V A that the wave functions $\varphi_\omega(z)$ and $\eta^{(\lambda)}(z)$ are, within the interaction region and at low energies E and E_{out}, proportional to $\sqrt{E}$ and $\sqrt{E_{\mathrm{out}}}$, respectively,

$$\varphi_\omega(z) = k_\perp \bar{\varphi}(z), \quad \eta_\lambda(z) = \frac{k_{\perp,\mathrm{out}}}{2}\bar{\eta}(z), \tag{5.11}$$

where $k_{\perp,\mathrm{out}}=\sqrt{2m_I[E-\hbar\omega_m(k_r)]/\hbar^2}=\sqrt{k_\perp^2-2m_I\omega_m(k_r)/\hbar}$; $\bar{\eta}(z)$ is normalized according to the same conventions as $\bar{\varphi}(z)$ as spelled out in Sec. V A, $\bar{\eta}(z)\to 2z$ for $z\to\infty$.

As above, the subscript r shall denote the lowest (ripplon or third sound) mode. Only film modes m of energy $\hbar\omega_m(k_r)<E$ can be excited. For films (as opposed to a free surface), energetically higher modes $m\neq r$ are separated by an energy gap from the third sound spectrum $m=r$ and cannot fulfill this inequality for sufficiently low incident E. Therefore, all modes $m\neq r$ can be ignored in the investigation of the $E\to 0$ limit.

The calculation of r_{inel} is a delicate matter since, in the low-momentum limit, $X_{r,k_r}(z)$ becomes very long ranged. Hence, we need a formulation that avoids large cancellations in the z integral for $M_r(\mathbf{k}_r,0)$. From the first of the two formulations (4.7), we find for perpendicular incidence

$$M_r(\mathbf{k}_r,0) = \frac{2m_I}{\hbar^2 k_{\perp,\mathrm{out}}}\frac{1}{2}\int dz \frac{\eta_\lambda(z)}{\sqrt{\rho_1^I(z)}}\{\epsilon_\lambda\varphi_\omega(z)-[H_1^I(z)\varphi_\omega(z)] - \varphi_\omega(z)H_1^I(z)\}\tilde{X}_{r,k_r}(z), \tag{5.12}$$

where $\epsilon_\lambda=|\mu_I|+E_{\mathrm{out}}$. The term $[H_1^I(z)\varphi_\omega(z)]$ is expressed in terms of the self-energy by using the equation of motion (4.8), and $H_1^I(z)\tilde{X}_{r,k_r}(z)$ can be expressed as [cf. Eq. (2.33)]

$$H_1^I(z)\tilde{X}_{r,k_r}(z) = -\left(\hbar\omega_r(k_r)+\frac{\hbar^2k_r^2}{2m_I}\right)\tilde{X}_{r,k_r}(z) - 2\tilde{V}_{r,k_r}(z). \tag{5.13}$$

Finally, using energy conservation [Eq. (4.21)], we find

$$M_r(\mathbf{k}_r,0) = \frac{2m_I}{\hbar^2 k_{\perp,\mathrm{out}}}\left[(\eta_\lambda|V_{r,k_r}|\varphi_\omega) + \frac{1}{2}\int dz dz'\,\eta_\lambda(z)X_{r,k_r}(z)\Sigma(z,z',0;-\mu_I)\varphi_\omega(z')\right]. \tag{5.14}$$

We have thus brought $M_r(\mathbf{k}_r,0)$ into a form where all integrands vanish for large z independent of k_r. For further discussion, we also need the long-wavelength behavior of the Feynman approximation for the third sound density oscillation $\phi_{r,k_r}(z)$. In Ref. 36, it was shown that, for $k_r\to 0$, $\phi_{r,k_r}(z)$ factorizes as

$$\phi_{r,k_r}(z) = -\sqrt{\frac{n\hbar k_r^2}{2m_B\omega_r(k_r)}}\mathbf{\Phi}_R(z) = -\sqrt{\frac{2n\hbar k_r^2}{m_B\omega_r(k_r)}}\frac{d\sqrt{\rho_1^B(z)}}{dn}, \tag{5.15}$$

with the third sound dispersion $\omega_r(k_r)\to c_3k_r$ for $k_r\to 0$. $\mathbf{\Phi}_R(z)$ is the shape of the long-wavelength density fluctuation. We have normalized it, deviating slightly from the conventions of Ref. 36, such that $\int dz\Phi_R(z)\sqrt{\rho_1(z)}=1$. A useful property of the ripplon or third sound shape function $\mathbf{\Phi}_R(z)$ can be derived from the rigorous expression for $\tilde{V}^I_{\text{p-h}}$,

$$V^I_{\text{p-h}}(\mathbf{r}_0,\mathbf{r}) = \frac{\delta V_H^I(\mathbf{r}_0)}{\delta\rho_1^B(\mathbf{r})} \tag{5.16}$$

and, hence,

$$\int d^3r V^I_{\text{p-h}}(\mathbf{r}_0,\mathbf{r})\frac{d\rho_1^B(\mathbf{r})}{dn} = \frac{dV_H^I(\mathbf{r}_0)}{dn}, \tag{5.17}$$

where we added the superscript B here to denote the background density. It is important to note again that Eq. (5.17) is true only in an exact theory, because the particle-hole interaction $V^I_{\text{p-h}}(\mathbf{r}_0,\mathbf{r})$ implies usually more diagrammatic approximations than $V_H^I(\mathbf{r}_0)$. The macroscopic derivatives on the right hand side of Eq. (5.17) is, therefore, more accurate than the two-point quantity on the left hand side.

The low-momentum behavior of $\tilde{X}_{r,k_r}(z_0)=\sqrt{\rho_1^I(z_0)}X_{r,k_r}(z_0)$ is now obtained from the normal-mode expansion (2.33),

$$\tilde{X}_{r,k_r}(z) = -2\sum_{\alpha} \frac{\eta^{(\alpha)}(z)}{\epsilon_\alpha + \hbar\omega_r(k_r) + \frac{\hbar^2 k_r^2}{2m_I}} (\eta^{(\alpha)}|\tilde{V}^I_{\text{p-h}}|\phi_{r,k_r}) = \sqrt{\frac{2n\hbar k_r^2}{m_B\omega_r(k_r)}} \sum_{\alpha} \frac{\eta^{(\alpha)}(z)}{\epsilon_\alpha + \hbar\omega_r(k_r) + \frac{\hbar^2 k_r^2}{2m_I}} \left(\eta^{(\alpha)}\sqrt{\rho_1^I}|\frac{dV_H^I}{dn}\right)$$

$$\to \sqrt{\frac{2n\hbar k_r^2}{m_B\omega_r(k_r)}} \left[\frac{\sqrt{\rho_1^I(z)}}{\hbar\omega_r(k_r)} \left(\rho_1^I|\frac{dV_H^I}{dn}\right) + \sum_{\alpha>0} \frac{\eta^{(\alpha)}(z)}{\epsilon_\alpha} \left(\eta^{(\alpha)}\sqrt{\rho_1^I}|\frac{dV_H^I}{dn}\right)\right] = \sqrt{\frac{2n\hbar k_r^2}{m_B\omega_r(k_r)}} \left[\frac{\sqrt{\rho_1^I(z)}}{\hbar\omega_r(k_r)} \frac{d\mu_I}{dn} + \frac{d\sqrt{\rho_1^I(z)}}{dn}\right] \tag{5.18a}$$

$$\to \sqrt{\frac{2nk_r^2}{m_B\hbar\omega_r^3(k_r)}} \frac{d\mu_I}{dn} \sqrt{\rho_1^I(z)} \quad \text{as } k_r \to 0, \tag{5.18b}$$

where

$$\left(\rho_1^I|\frac{dV_H^I}{dn}\right) = \frac{d\mu_I}{dn} \tag{5.19}$$

and

$$\sum_{\alpha>0} \frac{\eta^{(\alpha)}(z)}{\epsilon_\alpha} \left(\eta^{(\alpha)}\sqrt{\rho_1^I}|\frac{dV_H^I}{dn}\right) = \frac{d\sqrt{\rho_1^I(z)}}{dn} \tag{5.20}$$

are derived by differentiating the Hartree equation (2.29) with respect to background surface coverage n. The above result (5.18b) demonstrates our assertions that $X_{r,k_r}(z)$ is long ranged, in fact, independent of z, for vanishing k_r.

The first term of $M_r(\mathbf{k}_r,0)$ [cf. Eq. (5.14)] is a matrix element of the particle-hole potential $V^I_{\text{p-h}}(\mathbf{r},\mathbf{r}')$,

$$(\eta_\lambda|V_{r,k_r}|\varphi_\omega) = -\frac{k_\perp k_{\perp,\text{out}}}{2} \sqrt{\frac{\hbar k_r^2}{2m_B n\omega_r(k_r)}} V_r^{(\eta\varphi)}, \tag{5.21}$$

and, hence, we have for the full channel amplitude

$$M_r(\mathbf{k}_r,0) = -\sqrt{\frac{\hbar k_r^2}{2m_B n\omega_r(k_r)}} \frac{m_I k_\perp}{\hbar^2} \times \left[V_r^{(\eta\varphi)} - \frac{n}{\hbar\omega_r(k_r)} \frac{d\mu_I}{dn} M_r^{(\eta\varphi)}\right] \tag{5.22}$$

with

$$V_r^{(\eta\varphi)} = \left(\bar{\eta}\left| n\frac{dV_H^I}{dn}\right|\bar{\varphi}\right) \quad \text{and} \quad M_r^{(\eta\varphi)} = (\bar{\eta}|\Sigma(z,z',0;-\mu_I)|\bar{\varphi}). \tag{5.23}$$

Evidently, the second term in Eq. (5.22) dominates in the long-wavelength limit $k_r \to 0$. It is, therefore, the only term that needs to be retained in the further calculations for thin films.

The upper boundary Q of the momentum integration in Eq. (5.10) is determined by energy conservation: Q is the root of $E-\hbar\omega_r(k_r)-\hbar^2k_r^2/2m_I$, which, for low E, can be approximated by $Q \sim E/\hbar c_3$. Finally, we find for the inelastic scattering probability of slow particles hitting the ^{4}He film perpendicularly

$$r_{\text{inel}} \to k_\perp \left|\frac{d\mu_I}{dn}\right|^2 |M_r^{(\eta\varphi)}|^2 \left(\frac{m_I}{\hbar^2}\right)^2 \times \int_0^{E/\hbar c_3} \frac{dk_r}{2\pi} k_r \frac{n\hbar k_r^2}{2m_B c_3 k_r} \frac{1}{(\hbar c_3 k_r)^2} \sqrt{\frac{2m_I(E-\hbar c_3 k_r)}{\hbar^2}}$$

$$= k_\perp^4 \frac{n}{12\pi m_B} \frac{m_I}{m_B} \left|\frac{d\mu_I}{dn}\right|^2 \frac{|M_r^{(\eta\varphi)}|^2}{(\hbar c_3)^4} \tag{5.24a}$$

$$= \frac{1}{3\pi} E^2 \left(\frac{m_I}{\hbar^2}\right)^3 \left(\frac{m_B}{n\hbar^2}\right) \left|\frac{nd\mu_I/dn}{nd\mu_B/dn}\right|^2 |M_r^{(\eta\varphi)}|^2 \equiv r_{\text{inel}}^{(0)} E^2, \tag{5.24b}$$

where we have used for the last line $m_B c_3^2 = nd\mu_B/dn$. For very thick films, the n dependence of μ_I and μ_B is determined by the value of the substrate potential at the film surface; assuming a power law (for example, a van der Waals tail $\sim z^{-3}$) for both, the proportionality factor $r_{\text{inel}}^{(0)}$ appears to vanish with increasing film thickness as $1/n$. However, such a conclusion is premature because we can, for thick films, no longer neglect the first term in Eq. (5.22) and the second term in Eq. (5.18a). We will derive further below an interpolating expression for r_{inel} that covers the whole range from thin films to the free surface limit and shows that r_{inel} is always proportional to E^2 for $E \to 0$.

The result that the inelastic reflection coefficient is proportional to E^2 would not have been expected from superficial inspection of Eq. (5.10): A matrix element that remains finite as $k_r \to 0$ would lead to a behavior $r_{\text{inel}} \propto E^4$, but the divergence of the third sound contribution to the direct correlation $X_{r,k_r}(z)$ with vanishing parallel wave number k_r leads to $r_{\text{inel}} \propto E^2$. This divergence is known from the theory of impurities in bulk ^{4}He, where the coefficient of the $1/k$ singularity of the direct correlation function is directly connected with the *volume coefficient*, which is basically the ratio of the specific volumes of the impurity and a background particle.[23,37] In the present case, we can relate this singularity to the coverage dependence of the impurity

chemical potential, $d\mu_I/dn$. The second term of Eq. (5.14) describes the dynamic response of the film to the impinging particle. Our result that the self-energy is essential to describe the correct physics is analogous to the statement made in Ref. 3 that the self-energy is essential to obtain a nontrivial effective mass. Such an effective mass is likewise a direct consequence of the rearrangement of the background, which is, in that case, manifested in hydrodynamic backflow. In DWBA, the second term of $M_r(\mathbf{k}_r,0)$ as given by Eq. (5.14) is neglected altogether, because $\varphi_\omega(z)$ is replaced by $\eta_\omega(z)$. According to Eq. (5.10), r_{inel} in the DWBA is, therefore, proportional to E^4 instead of E^2. Unlike the DWBA of the sticking coefficient s, which yields the same energy dependence, albeit a different coefficient, the DWBA of r_{inel} leads to a qualitatively incorrect energy dependence.

A final word about the energy regime where Eq. (5.24a) is valid:

(1) We have assumed in the derivation of the low-energy properties that we are in the quantum reflection regime, i.e., the long-wavelength factorization (5.11) is valid. It is well known that long-ranged substrate potentials can reduce this regime to energies below 1 mK, and hence one should be cautious in applying Eq. (5.24a) for higher energies.

(2) It is straightforward to estimate the effect of the film thickness d: Typically, the linear third sound dispersion holds as long as the parallel wave number is less than the inverse film thickness, $k_r \ll d^{-1}$. The same is true for the low k_r behavior of the other ingredients $V_{r,k_r}(z)$ and $X_{r,k_r}(z)$. Hence, with increasing film thickness, and also with increasing incident energy E [but still low enough for condition (5.11) to be satisfied], there will be a crossover to a free surface behavior of r_{inel}. The free surface will be discussed in Sec. V C, and the crossover will be discussed in Sec. V D.

(3) Our derivations have always assumed that the particle-hole interactions $V_{\text{p-h}}(\mathbf{r},\mathbf{r}')$ and $V^I_{\text{p-h}}(\mathbf{r}_0,\mathbf{r})$ are the variational derivatives of the Hartree potentials $V_H(\mathbf{r})$ and $V^I_H(\mathbf{r}_0)$ with respect to the ^{4}He density. This is rigorously true only in an exact theory. Hence, some of the identities may be quantitatively violated in any approximate calculation. Therefore, we have formulated our results as far as possible in terms of density derivatives.

C. Low-energy inelastic reflection in the limit of a free surface

Here, we derive the inelastic reflection probability r_{inel} for a free ^{4}He surface and show how this limit is reached. There are three basic differences between a film surface and a free surface. First, the kinematic factors all change by changing the linear third sound dispersion relation to the ripplon dispersion relation

$$\omega_r^2(k_r) = \sigma k_r^3/m_B\rho_\infty, \tag{5.25}$$

where ρ_∞ is the bulk density and σ is the surface energy. Second, the sound modes within the background film become dense and it becomes energetically feasible to also excite sound waves that penetrate into the film, perpendicular to the free surface. These excitations have a *linear* dispersion law and, hence, are *above* the ripplon excitation, which should, therefore, remain the dominant energy loss mechanism for low energies; this is the basic assumption of this section. Third, the impurity chemical potential μ_I becomes independent of the ^{4}He film thickness; we must, therefore, expand the direct correlation $\tilde{X}_{r,k_r}$ in Eq. (5.14) to higher order in the ripplon wave vector.

The shape of the long-wavelength density oscillation in an infinite half-space follows directly from Eq. (5.15) and

$$\frac{d}{dn} \to -\frac{1}{\rho_\infty}\frac{d}{dz} \quad \text{as } n \to \infty. \tag{5.26}$$

Only the momentum-dependent normalization factor depends on the dispersion relation. Thus, we get the ripplon wave function and the particle-hole interaction[36]

$$\phi_{r,k_r}(z) = \sqrt{\frac{2\hbar k_r}{m_B\rho_\infty\omega_r(k_r)}}\frac{d\sqrt{\rho_1^B(z)}}{dz}$$

and

$$V_{r,k_r}(z) = \frac{1}{2}\sqrt{\frac{2\hbar k_r}{m_B\rho_\infty\omega_r(k_r)}}\frac{dV_H^I(z)}{dz}. \tag{5.27}$$

We can also determine $X_{r,k_r}(z)$ for small k_r, from Eq. (5.18a). The first term does not contribute in the free surface limit, hence

$$\tilde{X}_{r,k_r}(z) = \sqrt{\frac{2\hbar k_r}{m_B\rho_\infty\omega(k_r)}}\frac{d\sqrt{\rho_1^I(z)}}{dz}. \tag{5.28}$$

With these expressions for the long-wavelength limits of $V_{r,k_r}(z)$ and $X_{r,k_r}(z)$, the channel amplitude can be determined from Eq. (5.14). Since both $V_{r,k_r}(z)$ and $X_{r,k_r}(z)$ have now the same k_r dependence for $k_r \to 0$ [cf Eqs. (5.27) and (5.28)], both contribute to the low-energy limit of $r_{\text{inel}}(E)$:

$$M_r(\mathbf{k}_r,0) = \frac{m_I k_\perp}{\hbar^2}\sqrt{\frac{\hbar k_r}{2m_B\rho_\infty\omega_r(k_r)}}M_r^{(0)}(\infty) \tag{5.29}$$

with

$$M_r^{(0)}(\infty) = \int dz\,\bar{\eta}(z)\frac{dV_H(z)}{dz}\bar{\varphi}(z) + \int dz dz'\,\bar{\eta}(z)\frac{\eta^{(0)}(z)}{\eta^{(0)}(z)}\tilde{\Sigma}(z,z',0;-\mu_I)\bar{\varphi}(z'). \tag{5.30}$$

This yields for r_{inel} the low-energy limit

$$r_{\text{inel}} = \frac{k_\perp}{2\pi}\int dk_r k_r k_{\perp,\text{out}}\frac{\hbar k_r}{2m_B\rho_\infty\omega_r(k_r)}\left(\frac{m_I}{\hbar^2}\right)^2|M_r^{(0)}(\infty)|^2 = \frac{2}{9\pi}\left(\frac{m_I}{\hbar^2}\right)^3|M_r^{(0)}(\infty)|^2\left(\frac{E}{\sqrt{\sigma}}\right)^2. \tag{5.31}$$

To get the DWBA for the free surface, we must replace $\bar{\varphi}(z)$ by $\bar{\eta}(z)$ and keep only the first term of $M_r^{(0)}(\infty)$. Partial integration and using Eqs. (2.29) and (5.11) yield for $M_r^{(0)}(\infty)$

$$M_r^{(0)}(\infty) = \int dz \frac{dV_H(z)}{dz} [\bar{\eta}(z)]^2$$
$$= -\frac{\hbar^2}{m_I} \int dz \frac{d^2\bar{\eta}(z)}{dz^2} \frac{d\bar{\eta}(z)}{dz} = -\frac{\hbar^2}{2m_I} \left[\frac{d\bar{\eta}(z)}{dz} \right]^2_{z\to\infty}$$
$$= -2\frac{\hbar^2}{m_I},$$

where we used the asymptotic behavior $\bar{\eta}(z) \to 2z$. That is, the matrix element, and thus the inelastic reflection probability, for low energy depends only on the surface energy, but is independent of the structure of the surface

$$r_{\text{inel}} = \frac{8}{9\pi} \frac{m_I}{\hbar^2} \left(\frac{E}{\sqrt{\sigma}} \right)^2 \quad \text{(DWBA)}. \tag{5.32}$$

Such a simple result depending only on a static quantity, namely, the surface energy σ, has also been obtained for small angle inelastic scattering for perpendicular incidence on finite temperature films[38,39] (see also the next section). The inclusion of dynamic effects in Eq. (5.31) introduces a dependence of $r_{\text{inel}}(E \to 0)$ on the dynamic quantities of the scattering process: the scattering wave function $\bar{\varphi}$ and the self-energy $\Sigma(z,z',0;-\mu_I)$.

D. Low-energy limit of r_{inel} for thick films

Although we have a quadratic energy dependence, $r_{\text{inel}} \propto E^2$, for both scattering at thin films and at the free surface, the proportionality factors are different. In order to obtain the dependence of $r_{\text{inel}}(d)$ on the film thickness d up to $d \to \infty$, we take a closer look at the low-momentum limit of the quantities entering Eq. (5.10). The ripplon wave functions, Eqs. (5.15) and (5.27), are limits of the interpolating formula

$$\phi_{r,k_r}(z) = -\rho_\infty \sqrt{\frac{2\hbar k_r \tanh k_r d}{m_B \rho_\infty \omega_r(k_r)}} \frac{d\sqrt{\rho_1^B(z)}}{dn}, \tag{5.33}$$

with the interpolation for the surface wave dispersion[40]

$$\hbar^2 \omega_r^2(k_r) = \left(\frac{\hbar^2 c_3^2}{d} + \frac{\hbar^2 k_r^2}{2m_B} \frac{2\sigma}{\rho_\infty} \right) k_r \tanh k_r d. \tag{5.34}$$

Equation (5.15) is obtained by letting $k_r \to 0$ with d fixed, and Eq. (5.27) is obtained by first taking the limit $d \to \infty$ with k_r small but finite.

For the calculation of $M_r(\mathbf{k}_r,0)$, we now have to retain both terms in Eq. (5.18a),

$$\tilde{X}_{r,k_r}(z) \to \sqrt{\frac{2\hbar k_r \tanh k_r d}{m_B \rho_\infty \omega_r(k_r)}} \left[-\frac{\rho_\infty}{\hbar \omega_r(k_r)} \frac{d\mu_I}{dn} \sqrt{\rho_1^I(z)} + \frac{d\sqrt{\rho_1^B(z)}}{dz} \right]. \tag{5.35}$$

This yields the channel amplitude

$$M_r(\mathbf{k}_r,0) = \frac{m_I k_\perp}{\hbar^2} \sqrt{\frac{\hbar k_r \tanh k_r d}{2m_B \rho_\infty \omega_r(k_r)}} M_r^{(0)}(d) \tag{5.36}$$

with

$$M_r^{(0)}(d) = M_r^{(0)}(\infty) - \frac{\rho_\infty}{2\hbar \omega_r(k_r)} \frac{d\mu_I}{dn} (\bar{\eta}|\Sigma(z,z',0;-\mu_I)|\bar{\varphi}), \tag{5.37}$$

which now is still k_r dependent [see Eqs. (5.22) and (5.30) for comparison]. With increasing film thickness d, the k_r range, where the second term in Eq. (5.37) dominates over the first due to its divergence $\propto k_r^{-1}$, shifts to smaller values, because the coverage dependence of the chemical potential μ_I decreases. The inelastic scattering probability for any large but finite thickness d is

$$r_{\text{inel}}(E,d) = \frac{k_\perp}{2\pi} \int dk_r k_r k_{\perp,\text{out}} \frac{\hbar k_r \tanh k_r d}{2m_B \rho_\infty \omega_r(k_r)} \left(\frac{m_I}{\hbar^2} \right)^2 |M_r^{(0)}(d)|^2. \tag{5.38}$$

The behavior of $M_r^{(0)}(d)$ leads to a corresponding behavior of $r_{\text{inel}}(E,d)$: with increasing d, the E range, where the atom is scattered by third sound as described in the previous section, shifts to lower values; for energies above, the inelastic scattering probability $r_{\text{inel}}(E,d)$ is that of a free film, because the ripplons of shorter wavelength are excited, which do not "see" the finite depth of helium below the surface. In both these energy ranges, $r_{\text{inel}}(E,d) \propto E^2$, but the proportionality constants are different.

E. Small angle inelastic scattering

The discussion of inelastic small angle deflection from the specular direction (i.e., quasielastic scattering) of an impurity off a thin ^{4}He film is similar to the above discussion of inelastic scattering at low energies, because only long-wavelength third sound modes are excited. We restrict ourselves again, for simplicity, to perpendicular incidence, but the qualitative features of the conclusions are the same for any angle of incidence.

The probability $d\sigma_{\text{inel}}(\Omega)/d\Omega$ for inelastic scattering into a solid angle $d\Omega$ characterized by azimuthal and polar angles $\Omega = (\theta, \phi)$ is given by Eq. (4.35), where for perpendicular incidence, $d\sigma_{\text{inel}}(\Omega)/d\Omega$ does not depend on ϕ. The contribution from third sound is

$$\frac{d\sigma_r(\theta)}{d\Omega} = \frac{1}{4\pi^2} \sum_i \frac{\cos\theta k_{\text{out}}^2}{|1 + \hbar \omega_r'(k_r^{(i)}) \mathbf{k}_r \cdot \mathbf{k}_{\parallel,\text{out}}/k_{\text{out}}^2|} \frac{k_{\text{out}}}{k_\perp} |M_r(\mathbf{k}_r^{(i)},0)|^2, \tag{5.39}$$

where $M_r(\mathbf{k}_r^{(i)},0)$ is given by Eq. (5.14). For perpendicular incidence, there is only one solution $k_r^{(0)}$ of the equation

$$E - \hbar \omega_r(k_r) - \frac{1}{\sin^2\theta} \frac{\hbar^2 k_r^2}{2m_I} = 0, \tag{5.40}$$

which follows from energy and momentum conservation. For small angle scattering, we have $\theta \to 0$, $k_r^{(0)} \to k_\perp \sin\theta$, and $k_{\perp,\text{out}} \to k_\perp$. In this limit, Eq. (5.39) simplifies to

$$\frac{d\sigma_r(\theta)}{d\Omega} \to \frac{k_\perp^2}{4\pi^2}|M_r(k_\perp \sin\theta, 0)|^2. \tag{5.41}$$

We have already worked out the long-wavelength behavior of the third sound matrix element $M_r(k_r,0)$ in Sec. V B. For finite incident wave number $k_\perp$, the probability for quasielastic scattering off third sound modes becomes

$$\frac{d\sigma_r(\theta)}{d\Omega} \equiv \frac{1}{2\pi\sin\theta}\frac{d\sigma_r(\theta)}{d\theta} \to \frac{1}{4\pi^2}\frac{m_I}{m_B}\frac{2m_I}{\hbar^2 k_\perp \sin\theta}\left|\frac{d\mu_I}{dn}\right|^2\frac{n}{(\hbar c_3)^3} \times \left|\int dz dz' \eta_{k_\perp}(z)\Sigma(z,z',0;\omega)\varphi_\omega(z')\right|^2. \tag{5.42}$$

$d\sigma_r(\theta)/d\Omega$ diverges as $1/\sin\theta$ [hence, $d\sigma_r(\theta)/d\theta$ is finite]; for all other channels m above the third sound mode, $d\sigma_m(\theta)/d\Omega$ remains finite [or vanishes exactly if the channel is closed, $E<\hbar\omega_m(0)$] and can, for small θ, be neglected compared to $d\sigma_r(\theta)/d\Omega$.

Similar to the low-energy limit of r_{inel} for films, the DWBA leads to a qualitatively different result for the third sound contribution to the angular distribution for quasielastic scattering: $d\sigma_r/d\Omega$ vanishes linearly with θ, because in DWBA only the first term of $M_r(k_r,0)$ [Eq. (5.14)] is retained, which has an additional proportionality to k_r relative to the second term [see, for example, Eq. (5.22)]. In other words, the DWBA for $d\sigma_r/d\Omega$ predicts a "hole" in the specular direction, instead of a divergence.

We finally also take the limit of low incident energy, $k_\perp \to 0$. Then Eq. (5.11) holds and Eq. (5.22) can be inserted in Eq. (5.42),

$$\lim_{\theta\to 0}\frac{d\sigma(\theta)}{d\theta} = \frac{k_\perp^3}{8\pi}\frac{m_I}{m_B}\frac{m_I}{\hbar^2}\left|\frac{d\mu_I}{dn}M_r^{(\eta\varphi)}\right|^2\frac{n}{(\hbar c_3)^3} \quad \text{as } k_\perp \to 0. \tag{5.43}$$

Comparison of this result with the low-energy limit of the scattering probability r_{inel} (5.23) shows that the latter vanishes faster with $k_\perp$:

$$\frac{d\sigma(\theta=0)}{d\theta} \propto k_\perp^3 \quad \text{and} \quad r_{\text{inel}} \propto k_\perp^4. \tag{5.44}$$

However, according to the definitions (4.31b) and (4.32), both quantities are related via

$$r_{\text{inel}} = \int d\theta \cos\theta \frac{d\sigma(\theta)}{d\theta}. \tag{5.45}$$

Equations (5.44) and (5.45) can only be fulfilled simultaneously if the width of the angular distribution $d\sigma(\theta)/d\theta$ is of order $k_\perp$, i.e., the inelastic scattering probability distribution of low-energy impurities at ^{4}He films is sharply peaked in the specular direction. A similar behavior was also found in Ref. 38, where the DWBA was used at finite temperatures, because the spurious hole in the specular direction found in the DWBA is very small with increasing film thickness and the general feature that the reflected atoms are strongly peaked in specular direction[41] is consistent with both our calculation and that of Ref. 38.

VI. RESULTS

We consider thin films of liquid ^{4}He adsorbed on a plane attractive substrate which is translationally invariant in the x-y plane, i.e., $U_{\text{sub}}(\mathbf{r})=U_{\text{sub}}(z)$. The systems under consideration are characterized by a van der Waals substrate potential whose long-range part $U_{\text{sub}}(z)\to -C_3/z^3$ is, as we shall see, crucial for low-energy scattering properties in the millikelvin range. Our films are parametrized by the surface coverage n [Eq. (4.1)]. The density profile $\rho_1(z)$ is, along with the ground-state energy, structure functions, and Feynman modes of the film, obtained through the optimization of the ground state (2.1) as outlined in Sec. II A, and in much more detail in our previous work.[24,42] However, unlike in earlier work, where the dependence of the features of the films on the potential has been studied explicitly, we have chosen here the nuclepore substrate discussed extensively in Ref. 42. The ground-state correlations of the impurity atoms are, for very thick films, fairly independent of the details of the substrate potential; we will return to the question of the impurity-substrate interaction momentarily.

The H-He potential has been the subject of several *ab initio* calculations. Jochemsen *et al.*[43] have discussed the available potentials, measured the diffusion of H in He gas at low temperature, and proposed a potential (R2) which has become the *de facto* standard for atomic hydrogen researchers. However, Jochemsen *et al.* themselves preferred to use the older potential of Das *et al.*,[44] which is essentially the same as R2. For the sake of simplicity, we have, however, used the Lennard-Jones 6-12 potential by Toennies *et al.*;[45] we have compared the results, in the bulk liquid, with those obtained from the potential of Ref. 44 and found that the binding energies differ by less than 5%.

A. Static structure

We have carried out a sequence of ground-state calculations for our model of a helium film adsorbed on a nuclepore substrate,[24] with a coverage up to $n=0.39$ Å^{-2}, corresponding to about six liquid layers or to a thickness of $d=19$ Å, where d is defined as the first minimum of $d\rho_1(z)/dz$ coming from the vacuum side. d is only meaningful for films where the surface profile has reached its asymptotic form, while for nuclepore-adsorbed films of three or less atomic layers, d and n are not proportional.

For the ^{3}He-substrate interaction, we have taken the same potential as for the ^{4}He background. For the H-substrate interaction, a standard 3-9 potential was chosen

$$U_{\text{sub}}^I(z) = \frac{4}{27}\frac{C_3^3}{D^2}\frac{1}{z^9} - \frac{C_3}{z^3} \tag{6.1}$$

that is characterized by the well depth D and the van der Waals constant C_3. The parameters were estimated, using Ref. 46, to be $C_3=4400$ K Å^3 and $D=500$ K. The potential was supplemented, as described in Ref. 24, by the interaction

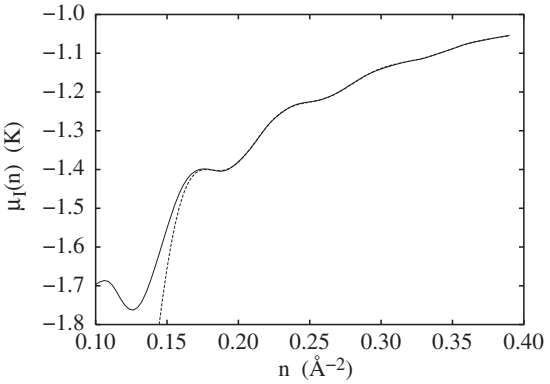

FIG. 3. The figure shows the chemical potential of a H impurity as a function of ^{4}He coverage (solid line). Also shown is the fit of the chemical potential by the functional form (6.2) generated from the numerical data in the coverage regime $0.18\ \text{Å}^{-2} \leqslant n \leqslant 0.38\ \text{Å}^{-2}$ (dashed line).

of the H atom with two solid layers of He, interacting via a Lennard-Jones 6-12 potential with the parametrization of Ref. 45. Figure 3 shows an interesting feature that was already (albeit much less dramatically) observed for ^{3}He impurities: The effect of the bare substrate potential is, in the coverage regime studied here, still largely compensated by the many-body effects: Asymptotically, the hydrogen chemical potential should be determined by the asymptotic part of the substrate potential, which is not the case here. Figure 1 shows another facet of the same observation: The substrate potential seen by both the H and the ^{3}He impurity are largely dominated by the many-body induced potentials. Hence, starting at a coverage of $n=0.20\ \text{Å}^{-2}$, the energy of the ground state of the hydrogen impurity changes by only 0.4 K in the range between coverages of $n=0.20\ \text{Å}^{-2}$ and the thick film limit. We have also used, for comparison, $U^I_{\text{sub}}(z)=0$ and found, consistent with the above observations, that the impurity ground-state properties are dominated, for $n \geqslant 0.20\ \text{Å}^{-2}$, by the features of the helium surface. We should stress that this does *not* imply that the scattering properties are independent of the impurity-substrate interaction; in fact, we will see that the opposite is true, especially for low scattering energies.

We need to point out a subtlety in connection with the ground-state calculations of both the background film and the ^{3}He impurity. Our low-energy results for r_{inel} contain ratios of the third sound velocity $m_B c_3^2 = n d\mu_B/dn$ and the coverage dependence of the impurity chemical potential, $n d\mu_I/dn$ [cf. Eq. (5.24)]. Both of these terms go to zero as the film grows. However, as pointed out previously, relations like Eqs. (2.13) and (5.16) hold only in an exact theory. To overcome this problem, we have slightly modified, as described in Ref. 42, the triplet corrections to the particle-hole interactions in the regime $0 \leqslant k_\parallel \leqslant 0.4\ \text{Å}^{-1}$ such that the speed of sound derived from the long-wavelength limit of the excitations agrees with the hydrodynamic speed of sound, $n d\mu_B/dn$, derived by numerically differentiating the chemical potential. Likewise, we have modified the impurity particle-hole interaction such that Eq. (5.19) is exactly satisfied. These modifications had no noticeable consequences on the ground-state energetics and structure. The chemical potentials were fitted by the analytic form for $i \in \{B, I\}$

$$\mu_i(n) = \mu_i(\infty) - \frac{\alpha_s \bar{\rho}^3}{n^3} + \frac{c}{n^4} + \frac{d}{n^5} + \frac{e\cos(kn-\gamma)}{n^4}. \quad (6.2)$$

The numerical values for the relevant parameters for ^{4}He and ^{3}He are given in Ref. 42.

In the calculation of the ground-state properties of the hydrogen impurity, we have omitted for efficiency triplet calculations, which comprise a major computational effort. *A posteriori* justification is found in the smallness of the "correlation hole" of the H atom, and in the small correction from elementary diagrams which is less than 0.05 K. Figure 3 shows the chemical potential of a single H atom as a function of ^{4}He coverage. We have fitted this chemical potential in the regime $0.18\ \text{Å}^{-2} \leqslant n \leqslant 0.39\ \text{Å}^{-2}$ with the analytic form (6.2). The fit, also shown in Fig. 3, predicts an asymptotic chemical potential of $\mu_I(\infty) \approx -0.93$ K, independent of the range of data that were used for the fit. This asymptotic value is in reasonable agreement with the experimental data between -0.89 ± 0.07 K (Ref. 17) and -1.15 ± 0.05 K.[16] Most of the other parameters depend, on the other hand, sensitively on the range of data used; they are, therefore, not very meaningful. Figure 3 also shows the value of the bare substrate potential at the location of the hydrogen bound state; evidently, this has little in common with the potential actually seen by the H atom.

The impurity ground states are shown, for a hydrogen and for a ^{3}He atom, in Fig. 1. The figures also shows the ^{4}He background density as a reference, the effective potential $V^I_H(z)$, and the substrate potential $U_{\text{sub}}(z)$. The effective potential $V^I_H(z)$ highlights, more than the binding energy or the shape of the ground state, the difference between the helium and the hydrogen impurities: While the hydrogen impurities have to overcome a rather steep potential step to intrude into the film, such a potential step is obviously absent in the case of ^{3}He.

It is interesting to know the H-He pair-distribution function for H physisorbed on ^{4}He. This is relevant in calculations of the optical spectrum for physisorbed H; for example, one can also use it to calculate the hyperfine frequency shift.[47,48] There are two ways to look at the pair-distribution function which give, while related, different pieces of information. The starting quantity is the general pair distribution (2.32) which is, in our geometry, a function of three variables

$$g^I(\mathbf{r}_0, \mathbf{r}) \equiv g^I(z_0, z, |\mathbf{r}_0^\parallel - \mathbf{r}^\parallel|). \quad (6.3)$$

The z_0 coordinate of the impurity should be taken at the average location of the impurity ground state; in other words, we define an average pair-distribution function, subject to the condition that the impurity is located in its ground state at $\mathbf{r}_{0,\parallel}=0$, as

$$\langle g^I \rangle(z, \mathbf{r}_\parallel) \equiv \int dz_0 \rho_1^I(z_0) g^I(z_0, z, |\mathbf{r}_\parallel|). \quad (6.4)$$

This average pair-distribution function describes the local environment of the impurity. Information on the distribution of ^{4}He atoms in the vicinity of the impurity is contained in

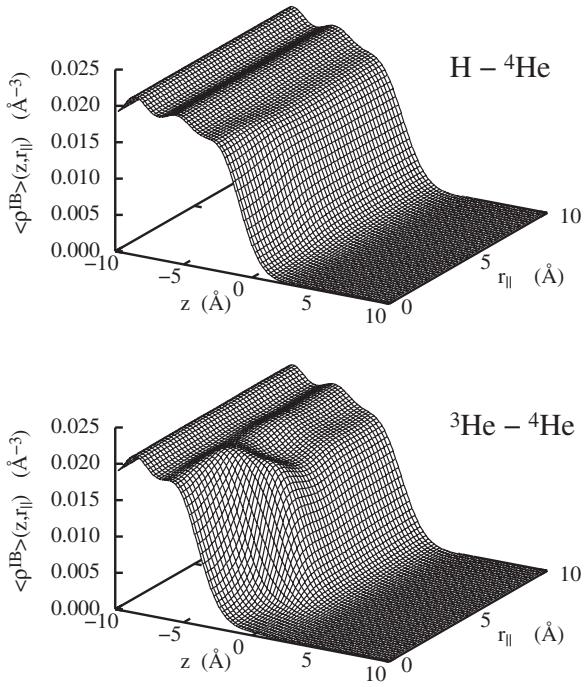

FIG. 4. The figure shows the correlation hole $\langle \rho^{IB} \rangle(z, r_\parallel)$ as defined in Eq. (6.5) around an impurity in its ground state for a H atom (upper figure) and a ^{3}He atom (lower figure). The underlying model is always a ^{4}He film with coverage $n=0.39$ Å^{-2}.

the averaged two-body density, which is the density of ^{4}He atoms

$$\langle \rho^{IB} \rangle(z, \mathbf{r}_\parallel) \equiv \rho_1(z) \langle g^I \rangle(z, \mathbf{r}_\parallel)$$
$$= \rho_1(z) \int dz_0 \rho_1^I(z_0) g^I(z_0, z, |\mathbf{r}_0^\parallel - \mathbf{r}_\parallel|). \quad (6.5)$$

The latter quantity is perhaps a little more illustrative; we, therefore, show $\langle \rho^{IB} \rangle(z, \mathbf{r}_\parallel)$ for the hydrogen and the ^{3}He impurity in Fig. 4.

B. Scattering: General discussion

We now turn to the main subject of this paper, namely, the calculation of scattering processes. We focus on inelastic processes; elastic scattering of ^{3}He off ^{4}He films has been discussed extensively in Ref. 3. We show in Figs. 5 and 6 the probabilities for the three types of scattering events off a film of coverage $n=0.36$ Å^{-2}, for a H and a ^{3}He atom impinging with wave vector $\mathbf{k}=(k_\perp, \mathbf{k}_\parallel)$, respectively:

(1) The elastic scattering probability $|R(\mathbf{k})|^2$ is determined by the coupling to *virtual* film excitations. After the interaction with the film, the atom leaves the film in a specular direction $(-k_\perp, \mathbf{k}_\parallel)$. Although a necessary condition for getting $|R(\mathbf{k})|^2 < 1$ is that the imaginary part of the self-energy is nonzero, it turns out that the value of the real part of the self-energy has a substantial effect on $|R(\mathbf{k})|^2$ as well as on the other two probabilities; it is *never* legitimate to ignore the real part of the self-energy.

(2) The inelastic scattering probability $r_{\text{inel}}(\mathbf{k})$, as defined in Sec. IV A, is the probability that the atom excites a third sound wave or other modes of the film, but still retains enough energy to leave the film.

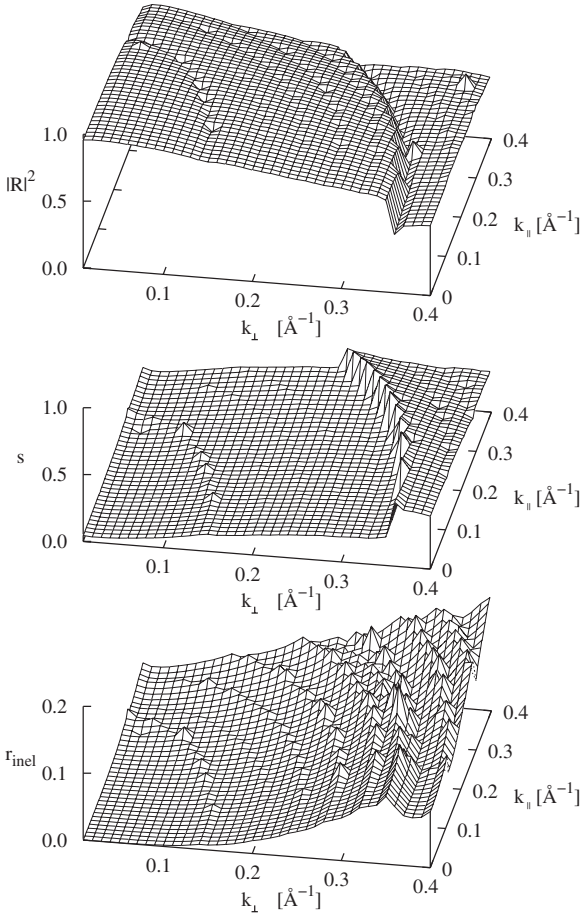

FIG. 5. The figure shows the elastic reflection probability $|R(k_\parallel, k_\perp)|^2$, the sticking probability $s(k_\parallel, k_\perp)$, and the inelastic reflection probability $r_{\text{inel}}(k_\parallel, k_\perp)$ of a H atom impinging on a ^{4}He film of coverage $n=0.360$ Å^{-2} as a function of the wave vector $\mathbf{k}=(k_\perp, \mathbf{k}_\parallel)$.

(3) The sticking coefficient $s(\mathbf{k})$ is the probability that the atom transfers a sufficient fraction of its kinetic energy plus the binding energy of the Andreev state—or other bound excited state in the case of ^{3}He scattering—to one or more film modes such that it becomes trapped at the ^{4}He surface.

The most obvious difference between H and ^{3}He is the steps in the H results for $|R(\mathbf{k})|^2$, $r_{\text{inel}}(\mathbf{k})$, and $s(\mathbf{k})$ as a function of momentum and scattering angle, as compared to smooth modulations in the ^{3}He results. As we will see below, the steps indicate the opening of a new decay channel. Concerning the modulations seen in ^{3}He scattering, we have shown in Ref. 3 for Cs-absorbed films that these modulations are shape resonances similar to those occurring for scattering at potential wells. The well associated with the self-consistent potential $V_H(\mathbf{r})$ grows with film thickness, accommodating an increasing number of states, leading to resonances. See also discussion in Sec. VI C.

Figures 5 and 6 also show that the limit of quantum reflection (at low energies, the reflection coefficient goes to unity) has, for the momenta shown, *not* yet been reached. For H scattering, the ^{4}He surface acts more like a wall, since it

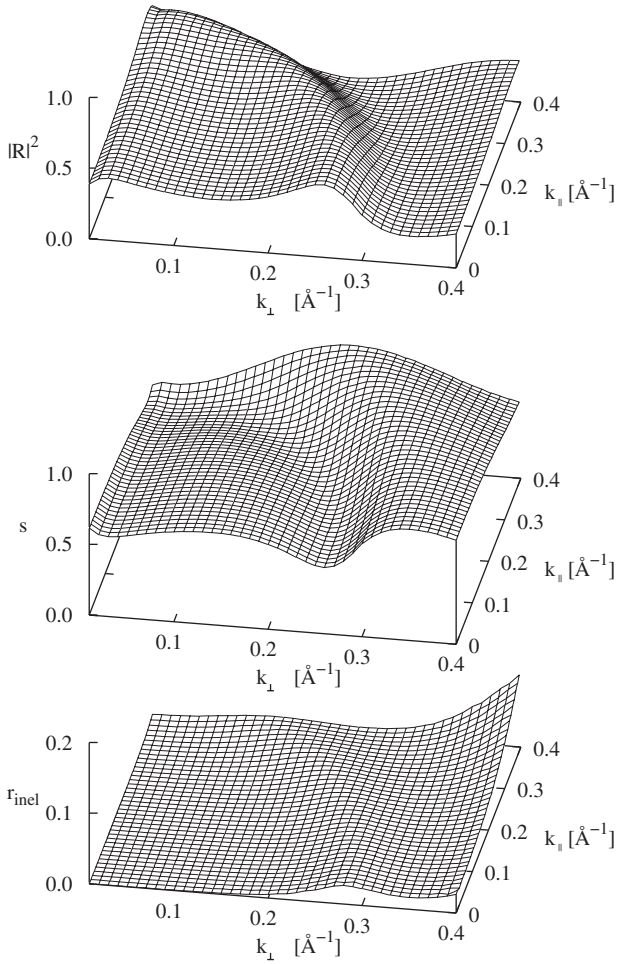

FIG. 6. Same as Fig. 5 for ^{3}He.

takes an energy of about 30 K of the H atom to penetrate into the bulk of the ^{4}He liquid (see Fig. 1). We must point out, however, that the manner in which the limit of quantum reflection is reached depends extremely sensitively on details of the density profiles.[49] Our results should, therefore, be considered with much caution.

For a deeper discussion of the inelastic processes involved in the present situation, we must take the excitation spectrum of the background film into account. Since we have used the Feynman approximation for the energies occurring in the energy denominator of the self-energy (3.13), we show in Fig. 7 the dynamic structure function $S(k_\parallel,\omega)$, for parallel momentum transfer, in Feynman approximation. The spectrum is discrete below the evaporation energy $|\mu_B|+\hbar^2k_\parallel^2/2m$. The figures also show $|\mu_B|-\hbar k_\parallel^2/2m_I$ for both ^{3}He and H. By energy conservation, its intersections with the Feynman modes give those modes that can be excited by an incident impurity atom that has asymptotically zero energy. Evidently, a low-energy H atom can excite only a surface excitation, but ^{3}He can couple to three different Feynman modes in the present example. Of course, the number of modes to which an atom can couple increases with the film thickness; the spectrum turns into a continuum in the infinite half-space limit.

Figure 8 shows $|R(E)|^2$, $r_{\rm inel}(E)$, and $s(E)$ of H and ^{3}He for perpendicular incidence up to energies of 8 K. For energies

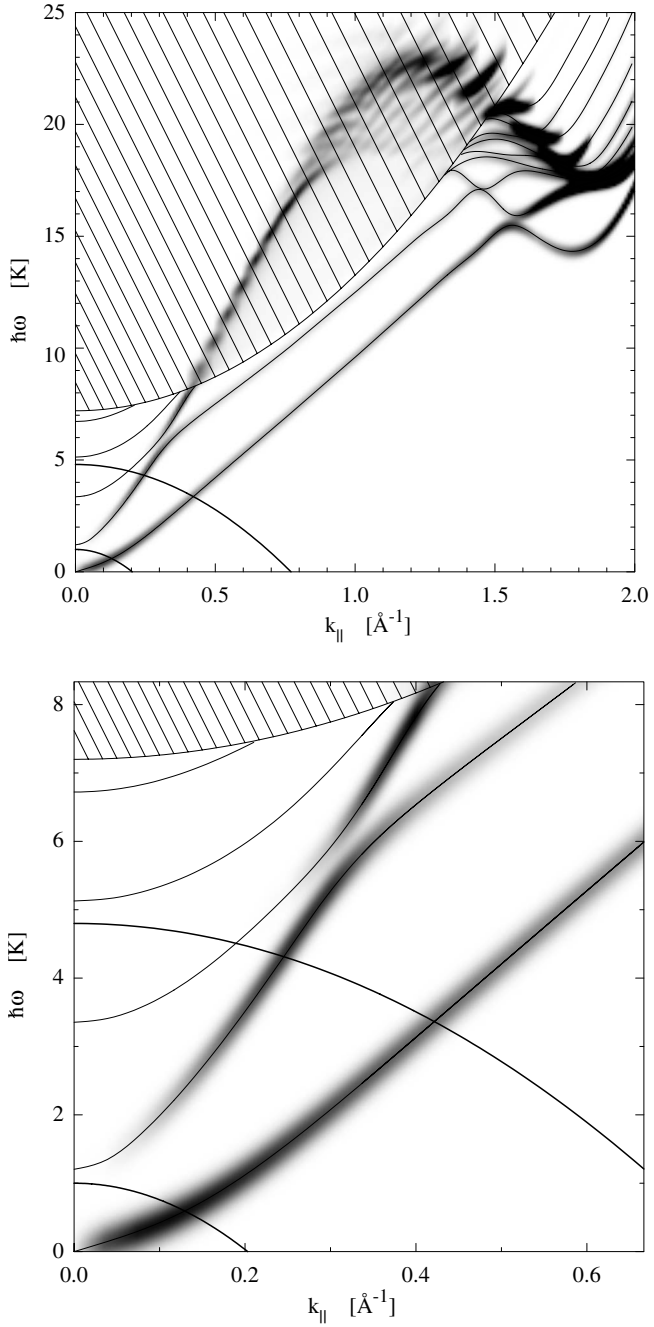

FIG. 7. The dynamic structure function $S(k_\parallel,\omega)$ for a film with $n=0.45$ Å^{-2} is shown in Feynman approximation. The excitations below the continuum (shown as hatched area) are discrete modes; $S(k_\parallel,\omega)$ has been broadened by a Gaussian of width 0.25 K to display their strength in gray scale. The two heavy lines are $|\mu_B|-\frac{\hbar^2k_\parallel^2}{2m_I}$ for ^{3}He (upper line) and H (lower line). Their intersections with the film dispersion yield the modes excited by ^{3}He or H scattering at zero energy by decay into the respective Andreev ground state. The lower panel is a magnification for low momentum and energy.

of several Kelvin, all three probabilities $|R|^2$, $r_{\rm inel}$, and s are of the same order of magnitude. The vertical lines indicate the threshold energies for decay channels $(\gamma=0,m)$, i.e., energies $E_{0,m}$, above which sticking by decay into the Andreev

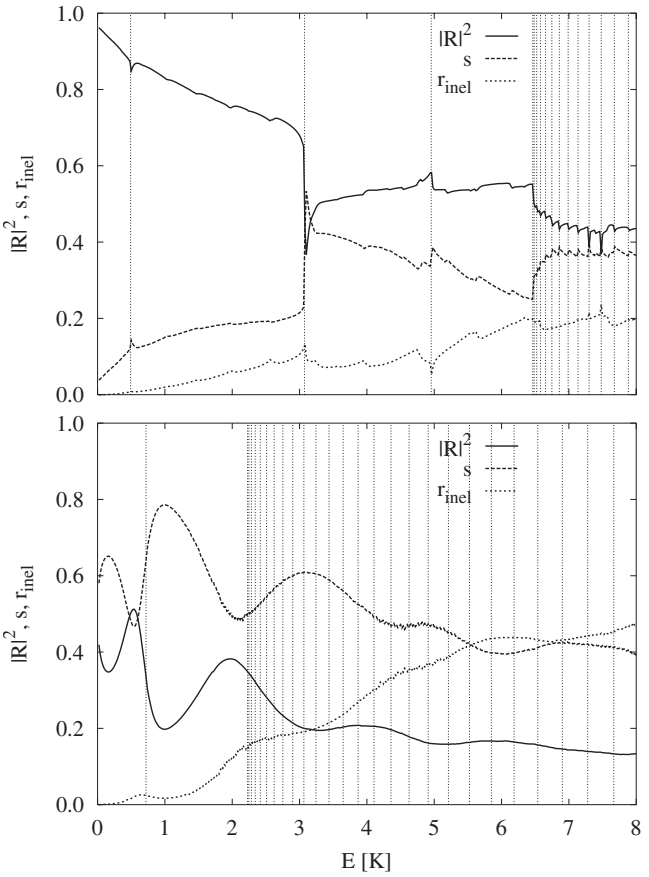

FIG. 8. The figures show the elastic (solid line) and inelastic (dashed line) reflection probabilities $|R(E)|^2$ and $r_{\mathrm{inel}}(E)$ as well as the sticking probabilities $s(E)=1-|R(E)|^2-r_{\mathrm{inel}}$ for perpendicular incidence of H (upper figure) and ^{3}He (lower figure) on a ^{4}He film adsorbed on nuclepore (coverage $n=0.360$ Å^{-2}). The threshold energies for channels associated with sticking are indicated by vertical lines; these lines become a continuum at $E=\mu_I-\mu$. The vertical lines within the continuum show the numerical discretization of the Feynman modes. Note that the limiting behavior $|R(E)|^2\to 1$ for $E\to 0$ is only reached at very low E and is not visible on the energy scale here.

ground state $\eta_0(z_0)$ and excitation of a film mode m is possible, $E_{0,m}=E+\mu_I-\hbar\omega_m(0)$ (see also Fig. 7). The spectrum is continuous for $\hbar\omega_m(0)$ larger than $\mu_B\approx 7.2$ K. For H, the passing of the incident energy E through one of the discrete energies $E_{0,m}$ has a major effect on $|R|^2$, r_{inel}, and s, leading to steps in all three quantities. As expected, s increases when such a new decay channel opens.

Of course, the phase space for multiexcitations increases with increasing energy, while the form of the self-energy (4.10) as well as the current (4.28) implies that decay into more than two elementary excitations is excluded. Therefore, corrections from multiexcitation processes are expected at high scattering energies.

C. Low-energy sticking of ^{3}He

The regime of validity of universal quantum reflection, $1-|R|^2\propto k_\perp$ as $\hbar k_\perp\to 0$, is determined, among others, by the proximity of low-lying resonances or shallow bound states of the impinging particle, which sees the long-ranged tail of the substrate potential, $-C_3/z^3$, and the effectively attractive or repulsive interaction with the film. Universal quantum reflection has been examined experimentally[6] as well as theoretically,[3,34,49] where it has been found that $1-|R|^2$ is, indeed, enhanced by the substrate potential and that the behavior $\propto k_\perp$ is shifted to lower energies, leading to an increased coefficient of the expansion of s in $k_\perp$,

$$s_1 \equiv \lim_{k_\perp\to 0}\frac{s(k_\perp)}{k_\perp}. \tag{6.6}$$

We will discuss in this and in the following section our results for the sticking probability.

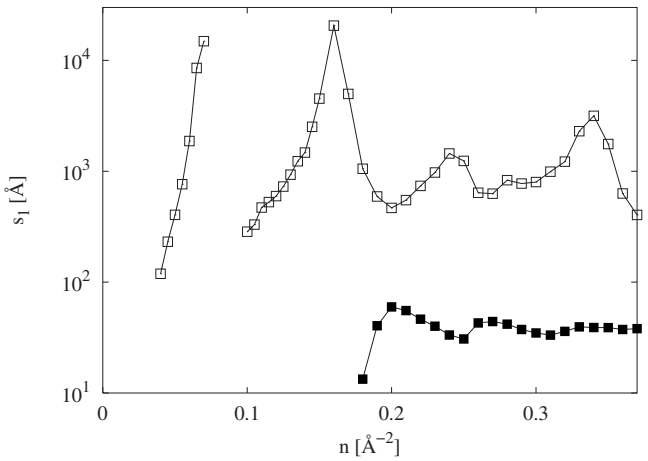

FIG. 9. The low-energy sticking coefficient of ^{3}He (open squares) and H (filled squares), divided by the incident perpendicular momentum $k_\perp$, $s_1=\lim_{k_\perp\to 0}\frac{s}{k_\perp}$, is plotted as a function of the coverage n of a ^{4}He film adsorbed on nuclepore.

Figure 9 shows $s_1(n)$ for ^{3}He scattered off ^{4}He films adsorbed on a nuclepore substrate, for the whole series of coverages n for which we have carried out calculations for ^{3}He. $s_1(n)$ for ^{3}He exhibits, as a function of surface coverage, a sequence of pronounced peaks. These peaks are the signatures of the appearance of additional bound states of ^{3}He in the film as its thickness increases. In Ref. 1, the following scenario was found as a function of surface coverage: The ground state of the ^{3}He impurity is, of course, always the Andreev state; this state is not renormalized by self-energy corrections $\Sigma_{\alpha\beta}(\omega)$ [cf. Eq. (3.12)]. As the film thickness increases, more bound states appear because ^{3}He impurities can be solvated in bulk ^{4}He with a solvation energy of approximately 2.7 K.[50] In the simple static approximation (2.29), the first excited state appears to be such a solvated state. If we include self-energy corrections and solve the full equation of motion (4.8) self-consistently for bound state wave functions $\varphi_\omega(z)$ with energies $\hbar\omega<-\mu_I$, then the first excited state becomes the second surface state observed in experiments,[51] whereas the third and all higher states describe ^{3}He atoms solvated in the ^{4}He background film. The density of these bound states increases with increasing n until they form a continuum of modes for the motion of ^{3}He

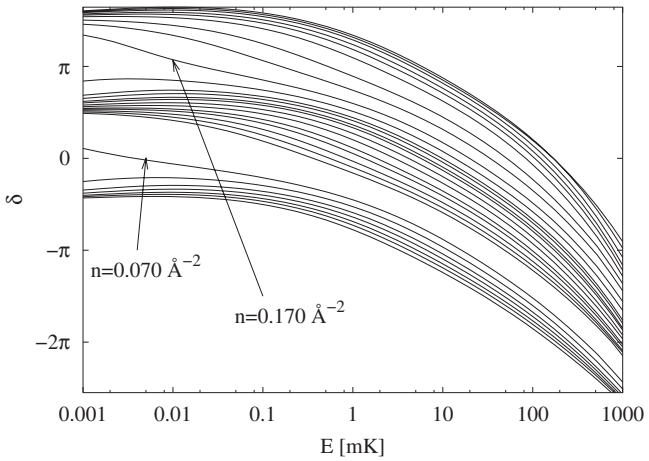

FIG. 10. The phase shift δ for ^{3}He scattering at films of coverages $n=0.040,\ldots,0.250$ Å^{-2} is shown as a function of incident energy E. δ rises monotonically from lowest to highest n. The π jumps at $n=0.070$ Å^{-2} and at $n=0.170$ Å^{-2} show the appearance of additional bound states and coincide with the peaks of the sticking coefficient s_1 at the same n (see Fig. 9). See text for a detailed discussion.

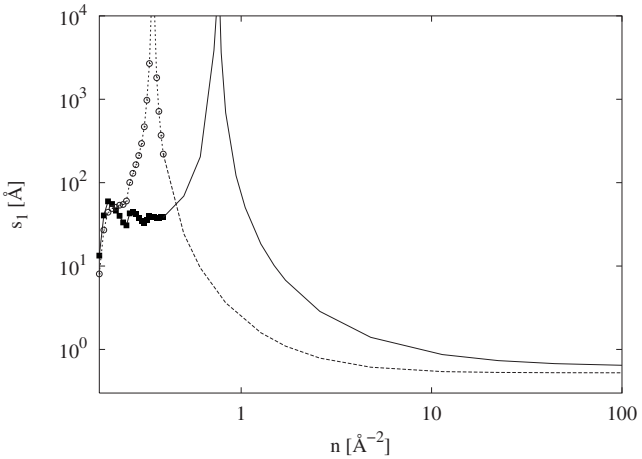

FIG. 11. s_1 is shown for H as a function of n, calculated directly for thin films up to $n=0.37$ Å^{-2} (filled squares, see also Fig. 9), while higher n are emulated as described in the text (full line). Also shown (circles and dashed line) is s_1 for H if retardation is taken into account.

solvated in bulk ^{4}He. Whenever a new bound state appears, the low-energy phase shift $\delta(E\to 0)$ of the elastic scattering amplitude $R=|R|e^{2i\delta(E)}$ jumps, in accordance with Levinson's theorem,[52] by π. This is shown in Fig. 10. These bound states are better approximations than the impurity states $\boldsymbol{\eta}^{(\alpha)}(\mathbf{r})$, and lie more densely because the ^{3}He impurity acquires an effective mass. Furthermore, all of these bound states are decay channels for sticking. However, since we have used the static approximation for the intermediate states, the sticking channels have somewhat different energies than those predicted by the self-consistent bound states of Eq. (4.8). In an exact theory, these energies would be the same.

We have also analyzed which processes contribute most to the low-energy sticking coefficient. While the relative contributions vary with coverage n, we found that, for all n, excitations of third sound modes is the main process leading to sticking, with the ^{3}He atom scattered either into the first or second Andreev state. From the thin films investigated here, we cannot yet draw conclusions for thicker films and the free ^{4}He surface, where sticking could also come from penetration into the ^{4}He bulk. Since even the six layer films examined here are evidently far from the bulk limit, an extrapolation to the infinite half-space is uncertain.

D. Low-energy sticking of H

The physics of H scattering is very different from that of ^{3}He scattering. Since hydrogen has a positive chemical potential [the HNC-Euler–Lagrange theory yields 31.6 K for H in bulk ^{4}He (Ref. 19 and 53)], the number of bound states does not increase with film thickness. Instead, for H, the ^{4}He surface acts almost like a hard wall (cf. Fig. 1). Since H is only very weakly bound to the ^{4}He surface, the third sound modes created in a sticking process of a low-energy H atom have a wave number of only about $k_0=0.13$ Å^{-1} (see Fig. 7). H is left with only a single channel for sticking to the ^{4}He surface, and has a much smaller sticking coefficent as compared to ^{3}He. This is evident in Fig. 9, which shows s_1 as a function of film coverage n for all nuclepore films for which we have carried out calculations for H. Furthermore, s_1 does not have the strong n dependence that we observed for ^{3}He, since no additional bound states are accommodated in the film as it grows.

Surface modes for the thickest film, $n=0.36$ Å^{-2}, with a wave number of k_0 and higher have already reached the free surface limit. It is, therefore, permitted to emulate thicker films as follows: We shift the substrate potential plus the H-He potential due to the solid first two ^{4}He layers toward the negative z direction and fill the resulting gap with homogeneous inert ^{4}He at equilibrium bulk density, $\rho_\infty=0.0218$ Å^{-3}. This procedure does not reproduce the layer structure close to the substrate correctly, but this does not compromise our results because these layer structures are immaterial for the binding properties of the H atom.

Due to the much stronger attraction of H to the nuclepore substrate than to an infinite half-space of ^{4}He, the H atom has, besides the Andreev ground state, for sufficiently thin films, a very weak *second* bound state with a binding energy in the millikelvin regime. This state is produced by the substrate attraction, whereas the Andreev state is produced by the interaction with the ^{4}He background. With increasing n, H is pushed away from the shallow well produced by the van der Waals tail $-C_3/z^3$ of the substrate, and the weakly bound state turns into a low-energy resonance. This is in contrast to ^{3}He, where the situation is reversed: There, resonances become bound bulklike modes with increasing n. However, in both cases, a resonance leads to an enhancement of the sticking coefficient s_1 by 1 or more orders of magnitude (see Fig. 11). In addition, Fig. 11 shows the result for the sticking coefficient if retardation, which weakens the long-range tail of the substrate potential, is taken into account, by multiplying the substrate potential by $\left(1+\frac{z}{\lambda}\right)^{-1}$, with $\lambda=200$ Å.[34] Retardation strongly influences low-energy results such as s_1, but does not lead to qualitative changes.

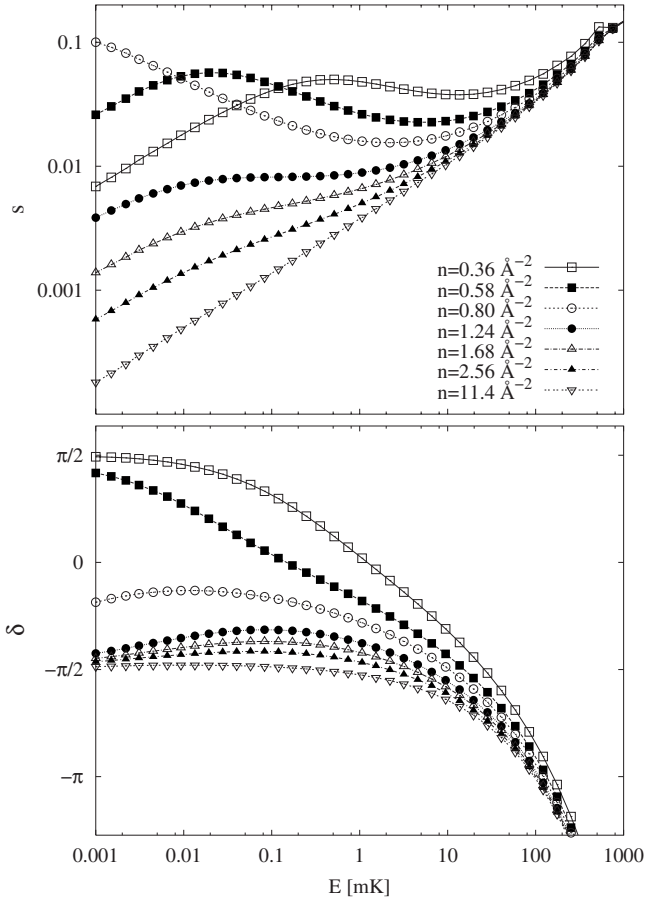

FIG. 12. The sticking coefficient $s(E)$ of H impinging perpendicularly on a ^{4}He film of coverage $n=0.36$ Å^{-2} and on thicker films (see text). The lower part of the figure shows the phase shift $\delta(E)$. When the weakly bound state of H becomes a resonance at $n=0.8$ Å^{-2}, $s_1=\lim_{k_\perp\to 0}\frac{s}{k_\perp}$ varies over several orders of magnitude and $\delta(E\to 0)$ jumps by π.

An effect which is similar to the resonant sticking enhancement is known for inelastic scattering of light atoms from solid surfaces, where it is called selective adsorption resonances (SAR). In particular, since resonant sticking here does not involve a reciprocal lattice vector due to translational symmetry parallel to the film, it corresponds to specular phonon-assisted SAR at low incident energy.[54,55]

Figure 12 shows the sticking coefficient $s(E)$ of H at the $n=0.36$ Å^{-2} film, which is about 17 Å thick, and for several thicker, emulated films up to $n=11.4$ Å^{-2} (approximately 520 Å thick). The phase shift $\delta(E)$, given by the argument of the elastic reflection coefficient $R=|R|e^{2i\delta}$, is shown in the lower part of the figure. Decreasing the film thickness from 1.24 to 0.80 Å^{-2} (from $d\approx 57$ Å to $d\approx 37$ Å), the phase shift $\delta(E\to 0)$ increases by π. As mentioned above, this jump of $\delta(E\to 0)$ is caused by the creation of weakly bound states when the effect of the nuclepore substrate on H is strong enough to accommodate a second bound state, in addition to the Andreev state.

In order to study the dependence of the scattering properties on the substrate, we have also looked at magnesium. In the upper panel of Fig. 13, we show the sticking coefficient

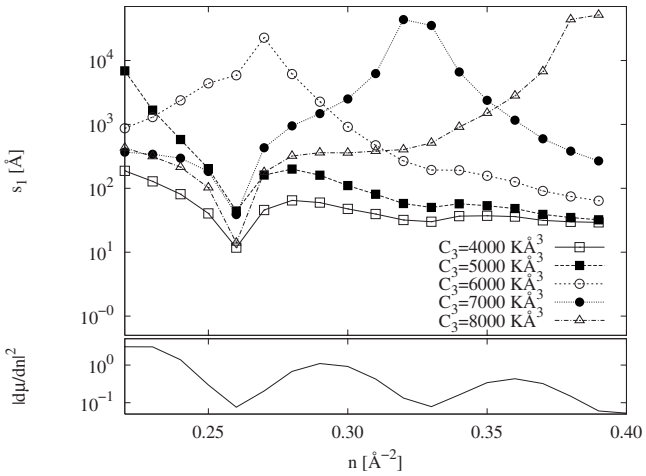

FIG. 13. The low-energy sticking coefficient of H, divided by the incident perpendicular momentum $k_\perp$, $s_1=\lim_{k_\perp\to 0}\frac{s}{k_\perp}$, is plotted as a function of the coverage n of a ^{4}He film adsorbed on magnesium, for different choices of the H-Mg van der Waals coefficient C_3. The lower panel shows $|d\mu_I/dn|^2$.

for H on magnesium-adsorbed ^{4}He films. The van der Waals constants C_3 for H interacting with an infinite Mg half-space was determined to be about 8000 K Å^3 in Ref. 56. However, for those substrates studied in Ref. 56 where independent calculations are available (see the review Ref. 46), we found a discrepancy of a factor of 2. For the ground-state calculation, we have chosen $C_3=4400$ K Å^3 and then carried out scattering calculations for van der Waals constants C_3 between 4000 and 8000 K Å^3.

Similar to H sticking on thick nuclepore-adsorbed films discussed above, there are clear signatures of resonances in the n dependence of s_1. In contrast to the nuclepore case, the resonance corresponds to the appearance of a *third* surface state of H. The dependence of the peak position on C_3 is easy to understand: with decreasing substrate strength C_3, the resonance peak moves to lower coverage n which allows the H atoms to come closer to the substate, thus compensating for the decrease of C_3.

s_1 exhibits oscillations apart from the resonance peak. This is best seen for the weakest $C_3=4000$ K Å^3, where no resonance is found in the n range shown in Fig. 13. The lower panel of Fig. 13 shows the n dependence of $|d\mu_I/dn|^2$ in comparison with s_1. In particular, the dip of s_1 for $n=0.26$ Å^{-2} is clearly correlated with a minimum of $|d\mu_I/dn|^2$. Unlike for $r_{\rm inel}$ which is proportional to $|d\mu_I/dn|^2$ [see Eq. (5.24b) and the discussion in the following section], this behavior is not immediately obvious from Eq. (5.7) for s_1, because it comes from the n dependence of the elastic channel wave function $\bar{\varphi}$.

E. Low-energy inelastic scattering

We have derived in Sec. V B a low-energy expansion for the inelastic reflection coefficient; specifically, it was shown that the dynamic response of the background film yielded $r_{\rm inel}=r^0_{\rm inel}E^2$, where the coefficient $r^0_{\rm inel}$ is given by Eq. (5.24b). This coefficient depends on the ratio of two num-

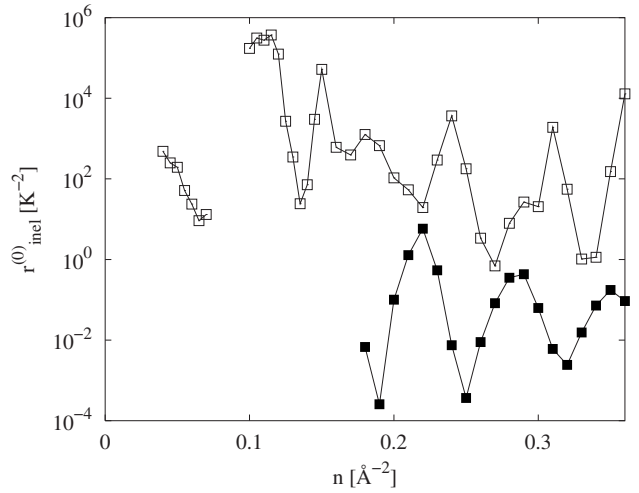

FIG. 14. The low-energy inelastic scattering probability divided by E^2, $r^{(0)}_{\text{inel}}=\lim_{E\to 0} r_{\text{inel}}/E^2$, is shown for ^{3}He (open squares) and H (filled squares) impinging perpendicularly on ^{4}He films of thickness n adsorbed on nuclepore.

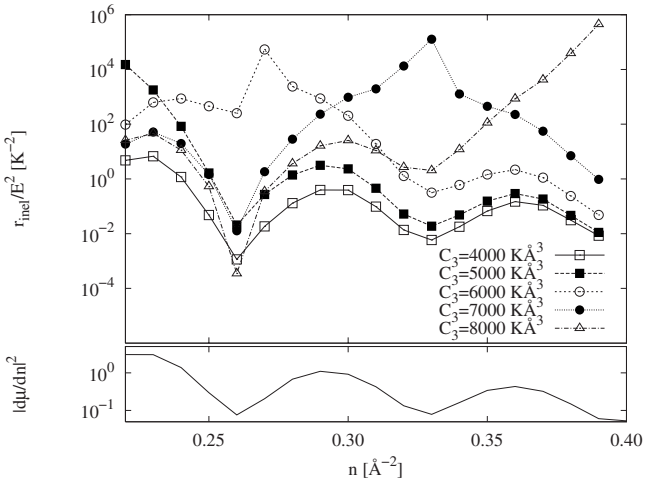

FIG. 15. In the upper panel, the low-energy inelastic scattering probability divided by E^2, $r^{(0)}_{\text{inel}}=\lim_{E\to 0} r_{\text{inel}}/E^2$, is shown for H impinging perpendicularly on ^{4}He films of thickness n adsorbed on magnesium, for different choices of the H-Mg van der Waals coefficient C_3. The lower panel shows $|d\mu_I/dn|^2$.

bers, $nd\mu^I(n)/dn$ and $nd\mu^B(n)/dn$, which both become small in the thick film limit.

A reliable microscopic calculation of this ratio from the particle-hole interaction $\tilde{V}_{\text{p-h}}(\mathbf{r},\mathbf{r}')$ and $\tilde{V}^I_{\text{p-h}}(\mathbf{r}_0,\mathbf{r})$ calculation of r^0_{inel} is difficult because the necessary integrations [for example, by Eq. (5.17) and a corresponding calculation for the background[36]] imply the cancellation of large numbers. For example, the *typical* order of magnitude of the particle-hole interaction appearing in Eq. (5.17), is $m_B c_s^2 \approx 25$ K, where c_s is the bulk speed of sound. Both $nd\mu^I(n)/dn$ and $nd\mu^I(n)/dn$ are, on the other hand, oscillating functions with values between 0.5 and 0.05 K in the coverage regimes 0.25 and 0.39 Å^{-2} and tend toward zero in the infinite half-space limit.[42] We have, therefore, calculated these quantities directly from our numerical chemical potentials.

In Fig. 14, we show the limit $r^{(0)}_{\text{inel}}=\lim_{E\to 0}(r_{\text{inel}}/E^2)$ as a function of n for ^{3}He and H scattering at ^{4}He films of coverage n. For H, the oscillations over several orders of magnitude are due to the numerator as well as denominator of the factor $|\frac{nd\mu_I/dn}{nd\mu_B/dn}|^2$ in Eq. (5.24b): $d\mu_I/dn$ and $d\mu_B/dn$ oscillate out of phase, and the ratio is enhanced. For ^{3}He, however, the strongly oscillatory n dependence is also partly caused by $M_r^{(\eta\varphi)}$, which also fluctuates as a function of coverage: $M_r^{(\eta\varphi)}$ depends on the zero-energy wave function of the elastic channel, $\bar{\varphi}(z_0)$, which for ^{3}He is sensitive to the size of the film due to the resonances occurring when successively more scattering states turn into bound states, i.e., fall below the zero-energy threshold. We have discussed these resonances in the previous section about the sticking coefficient. Being such a sensitive probe of the film thickness, $\bar{\varphi}(z_0)$ is also a sensitive probe of very small differences in the numerical convergence of the *independent* ground-state calculation of the films of different n. Therefore, some of the fluctuations of $M_r^{(\eta\varphi)}$ could also be caused by such numerical inconsistencies among films of different but close n.

In the upper panel of Fig. 15, $r^{(0)}_{\text{inel}}$ for H on Mg-adsorbed ^{4}He films is shown for different choices of C_3 (see explanation above). The behavior is similar to the n dependence of the sticking coefficient s_1, which is dominated by resonances due to the appearance of bound states. The oscillations of $|d\mu_I/dn|^2$ shown in the lower panel are responsible for the oscillations of $r^{(0)}_{\text{inel}}$; this is best seen for $C_3=4000$ K Å^3, where no resonance is found in the n range shown and where $r^{(0)}_{\text{inel}}$ is almost proportional to $|nd\mu_I/dn|^2$: for Mg, unlike for nuclepore, the denominator $|m_B c_3^2|^2=|nd\mu_B/dn|^2$ does not lead to an additional oscillatory behavior of $r^{(0)}_{\text{inel}}$, because c_3 is significantly larger for Mg and the relative variations of c_3 as the film grows are small. Hence, in the present case of Mg, and in the lower range of C_3, $r^{(0)}_{\text{inel}}$ is a direct and very sensitive probe of the coverage dependence of the impurity chemical potential.

In Sec. V D, we have derived an approximate inelastic scattering probability $r_{\text{inel}}(E,d)$ for thick films [Eq. (5.38)], making use of the phenomenological dispersion relation (5.34). For the numerical evaluation of $r_{\text{inel}}(E,d)$, we have resorted to using asymptotic properties and hydrodynamic derivatives. For the n dependence of chemical potentials $\mu_I(n)$ and $\mu_B(n)$, we took the asymptotic forms $\mu_{B,I}(d)=\mu_{B,I}(\infty)-C_3^{(B,I)}/d^3$, with $d=n/\rho_\infty$, valid for thick films only. We have taken for the calculation of the channel amplitude (5.37) the self-energy Σ and the Hartree potential V_H from the $n=0.36$ Å^{-2} film. This way we obtain an approximate probability which, however, retains the qualitative features of the E and d dependence of r_{inel}. In Fig. 16, $r_{\text{inel}}(E,d)$ is plotted for H scattering off thick films. Both sets of results show very clearly the fact that there are *two separate* regimes of quadratic behavior $r_{\text{inel}}(E,d)=\alpha E^2$ with *different* coefficients α; in the crossover regime, the energy dependence turns out to be quartic, $r_{\text{inel}}(E,d)\sim E^4$.

F. Inelastic cross sections

In this section, we present results for differential cross sections, i.e., the inelastic flux as a function of outgoing di-

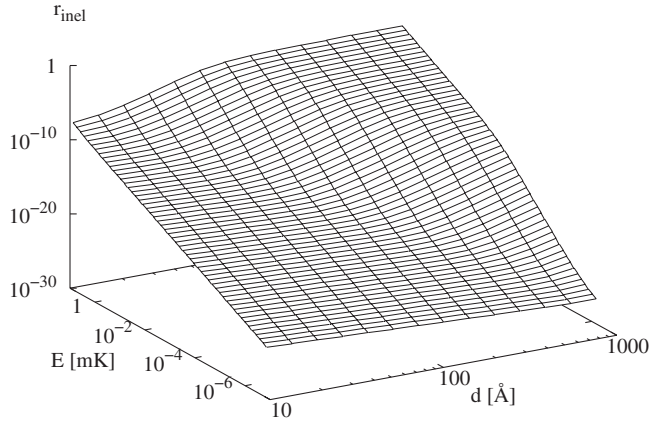

FIG. 16. The low-energy inelastic scattering probability $r_{\text{inel}}(d,E)$, shown as a function of the energy of the impinging H atom and of film thickness d, has two regimes of $r_{\text{inel}} \sim E^2$ dependence with different prefactors, separated by a regime where $r_{\text{inel}} \sim E^4$.

rection Ω, $\frac{d\sigma_{\text{inel}}(\Omega)}{d\Omega}$ [Eq. (4.35)], and as a function of outgoing perpendicular momentum $k_{\perp,\text{out}}$, $\frac{d\sigma_{\text{inel}}(k_{\perp,\text{out}})}{dk_{\perp,\text{out}}}$, i.e., the projection of Eq. (4.37) onto the z axis.

We start the discussion with the angular dependence of the inelastic flux in the limit of low incident energy, as derived in Sec. V E, where it was shown that the high probability for quasielastic reflection (direct inelastic scattering in almost specular direction) is a consequence of the coupling to the long-wavelength third sound modes of the ^{4}He film and closely connected to the E^2 proportionality of the total inelastic scattering probability. We show in Fig. 17 the angle dependent inelastic scattering cross section divided by k^3, $k^{-3}d\sigma(\theta)/d\theta$, for H and ^{3}He (using a logarithmic scale for the latter) impinging perpendicularly on the film with wave number k. Clearly, $\frac{d\sigma(\theta=0)}{d\theta}$ becomes proportional to k^3. The width of the scattering cone about the specular direction is proportional to k, as it is dictated by the behavior $r_{\text{inel}} \sim k^4$ for $k \to 0$. Hence, in the limit of low energies, the inelastic flux becomes increasingly focused in the specular direction, i.e., normal to the film in the present case, where we have restricted ourselves to normal incidence. The focusing in the specular direction would be the same for particles impinging at an arbitrary angle.

For finite incident energies, the cross section $\frac{d\sigma(\theta)}{d\theta}$ is shown in Fig. 18 up to incident energies of 8 K, again for perpendicular incidence. We observe that at energies on the order of Kelvin, the quasielastic scattering processes just discussed are negligible compared to deflection into finite angles θ. There is a striking difference between the results for H and ^{3}He, as the $\frac{d\sigma(\theta)}{d\theta}$ for the latter has clearly a much richer structure, with oscillations as function of the angle θ which become more numerous with increasing energy. The nature of these oscillations can be better understood by studying the cross section $d\sigma/dk_{\perp,\text{out}}$, defined by Eq. (4.37). Hence, we study the probability to scatter inelastically from an incoming state of wave number $k_{\perp,\text{in}}$ into an outgoing state of wave number $k_{\perp,\text{out}}$. In Fig. 19, $d\sigma/dk_{\perp,\text{out}}$ is plotted

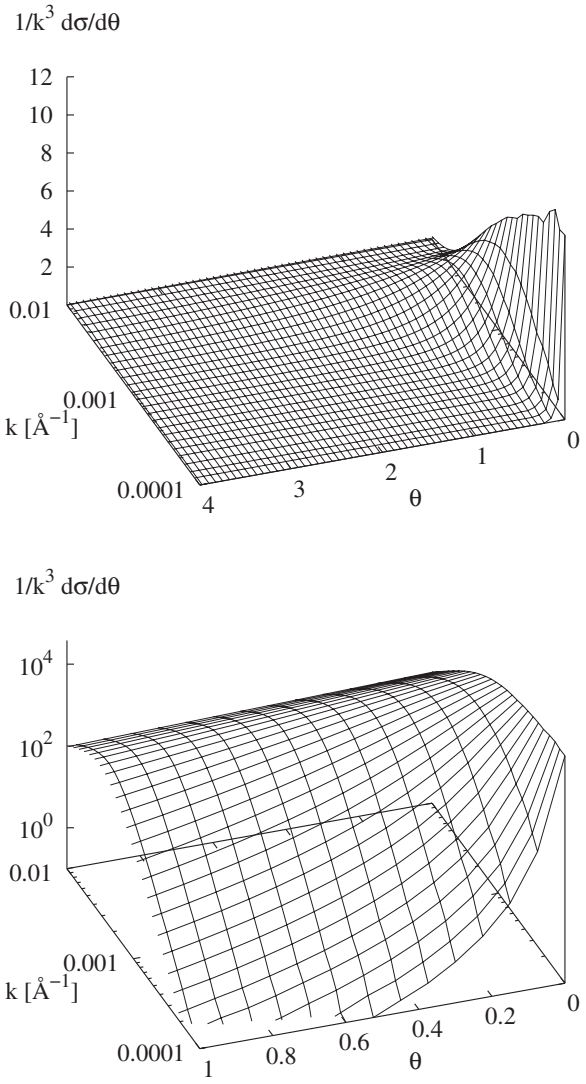

FIG. 17. The figure shows the differential inelastic scattering probability divided by k^3, $\frac{1}{k^3}\frac{d\sigma(\theta)}{d\theta}$, as a function of k, for perpendicular incidence of H (top) and ^{3}He (bottom) of incident wave number k on a ^{4}He film of coverage $n=0.360$ Å^{-2}. The wave number range $k=0.0001,\ldots,0.01$ Å^{-1} corresponds to an energy range $E=2.4\times10^{-7},\ldots,2.4\times10^{-3}$ K for H, and $E=8.1\times10^{-8},\ldots,8.1\times10^{-4}$ K for ^{3}He.

as a function of $k_{\perp,\text{in}}$ and $k_{\perp,\text{out}}$ for perpendicular incidence. Again, oscillations of the scattering probability are visible for ^{3}He. They can be attributed to interferences between the incoming and outgoing states in the transition matrix element $M_m(\mathbf{k}_m,0)$. Roughly speaking, these oscillations can be thought of as interference patterns stemming from the Fourier transform of the direct interaction $\nabla X_{m,k_m}(z_0)$ for wave number $k_{\perp,\text{in}}-k_{\perp,\text{out}}$, hence the approximately diagonal orientation of the oscillations. These oscillations will be distorted, because the channel wave functions are not simple plane waves and, furthermore, $\nabla X_{m,k_m}(z_0)$ changes with k_m, which is given by parallel momentum conservation. The wave number $k \approx 0.2$ Å^{-1} of these oscillations implies that the region of interaction between ^{3}He and third sound (the other film modes contribute negligibly to Fig. 19) is of the

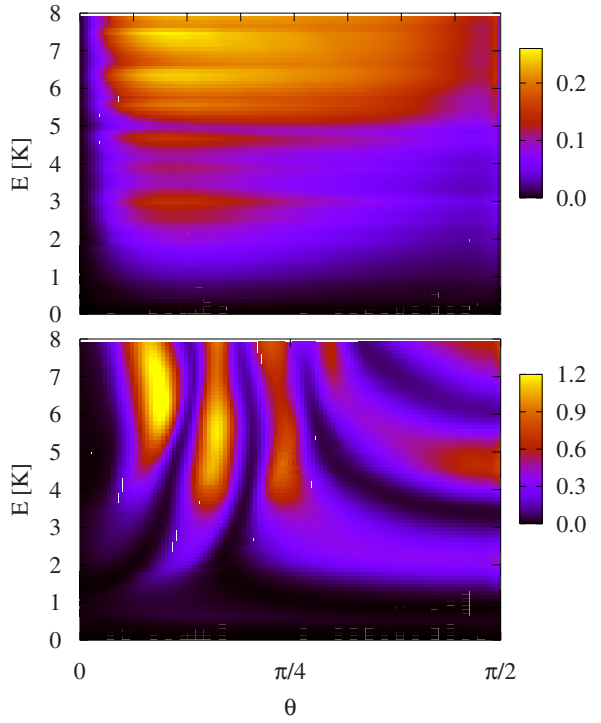

FIG. 18. (Color online) The angular dependence of the inelastic scattering probability $\frac{d\sigma(\theta)}{d\theta}$ is shown for H (upper panel) and for ^{3}He (lower panel) impinging with energies E perpendicularly on a ^{4}He film of coverage $n=0.360$ Å^{-2}.

order of $\frac{2\pi}{0.2}\approx 30$ Å, i.e., of the order of the film thickness. Turning now to the corresponding map for H scattering, we note that, due to the strong repulsion between H and the film, the ripplon interaction region is much smaller, leading to the much broader structure seen in the upper panel of Fig. 19. The increase of the cross section for $k_{\perp,\mathrm{in}}$ larger than about 0.43 Å^{-1} in Fig. 19, corresponding to $E\approx 5$ K in Fig. 18, is caused by the opening of an inelastic scattering channel (excitation of the film mode with perpendicular quantum number $m=3$; the opening of the $m=2$ channel at $k_{\perp,\mathrm{in}}\approx 0.25$ Å^{-1} is barely visible in Fig. 19).

The cross section $\frac{d\sigma(\theta)}{d\theta}$ in Fig. 18 reveals another interesting effect: for inelastic scattering into the direction almost parallel to the surface, $\theta\to\pi/2$, the scattering probability increases before it vanishes at $\theta=\pi/2$. This is the same effect as the suppression of quantum reflection caused by the long range of the van der Waals attraction of the substrate. Above we have seen that, in the elastic channel, this attraction leads to an increase of s at *small* incident energies. For direct inelastic scattering, it leads to an increase of scattering into large angles $\theta\to\pi/2$ at *any* incident energies, because at these angles the inelastic channel wave functions, asymptotically proportional to $e^{ik_{\perp,\mathrm{out}}z}e^{i\mathbf{k}_{\parallel,\mathrm{out}}\mathbf{r}_{\parallel}}$, have a small perpendicular momentum $k_{\perp,\mathrm{out}}$, just like the elastic channel wave function $\varphi(z_0)$ for low incident perpendicular momentum $k_\perp$. In other words, the resonance causes a high density of states in the film, leading, in the case of the elastic channel wave function, to a high probability for the impurity to generate a film mode, and, in the case of the inelastic channel wave functions, to a high probability to decay into that channel.

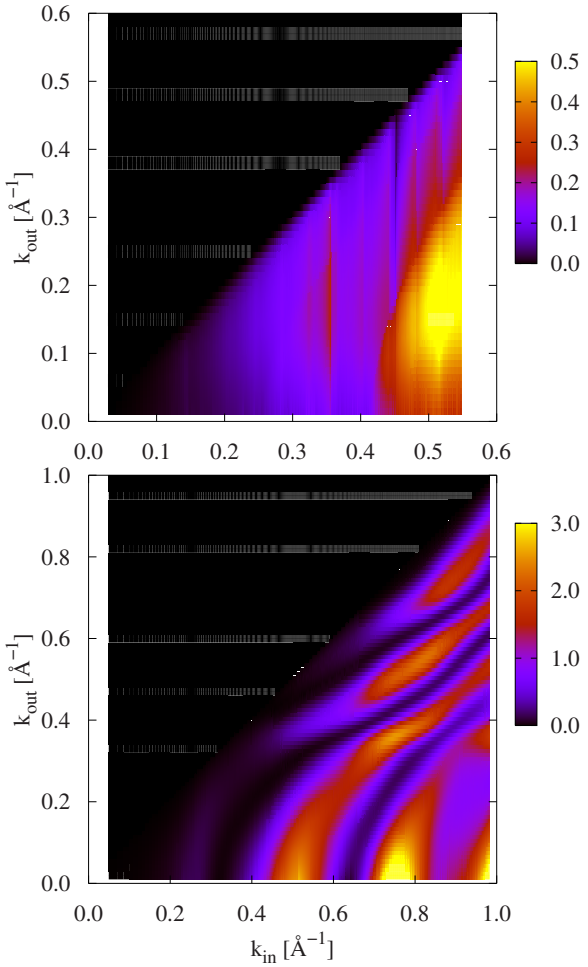

FIG. 19. (Color online) The inelastic scattering probability is shown, for H (top) and ^{3}He (bottom) impinging perpendicularly on a ^{4}He film ($n=0.360$ Å^{-2}), as a function of the initial wave number k_{in} (x axis) and of the perpendicular component of the final wave number $k_{\perp,\mathrm{out}}$.

This explanation for the peak of $\frac{d\sigma(\theta,k)}{d\theta}$ near $\theta=\pi/2$ is readily checked by comparing various film thicknesses, where films thicker than $n=0.36$ Å^{-2} are emulated as explained in Sec. VI D. In Fig. 20, $\frac{d\sigma(\theta,k)}{d\theta}$ for H is shown for increasing film thickness. Reaching about $n=0.80$ Å^{-2} (corresponding to a thickness $d\approx 37$ Å), the probability for inelastic scattering to $\pi/2$ increases dramatically, just as did s. For even thicker films, $\frac{d\sigma(\theta,k)}{d\theta}$ vanishes monotonously toward $\theta=\pi/2$.

This resonant scattering into the direction parallel to the film appears to be similar to *threshold resonances* for atom scattering at solid surfaces.[54,55] However, the underlying physics is quite different: in the latter case, threshold resonances occur also for elastic scattering due to translational symmetry breaking parallel to the surface which opens elastic channels, each associated with reprocal lattice vectors. Here, the effect happens at low energy in the *inelastic* scattering channel only if a weakly bound adsorption state is present.

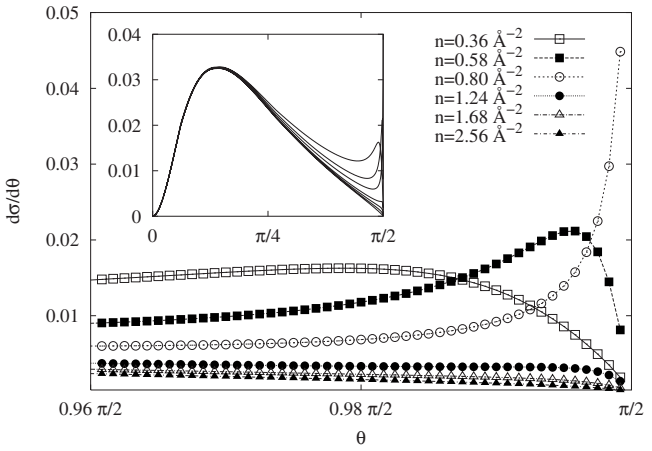

FIG. 20. $\frac{d\sigma(\theta)}{d\theta}$ is shown, for H impinging perpendicularly on ^{4}He films with energy $E=1.08$ K, for various film coverages. Near $\theta \rightarrow \pi/2$, the probability is enhanced by the low-energy resonance or weakly bound state of H, analogous to the enhancement of the sticking probability s, with a resonance for $n=0.8$ Å^{-2}, corresponding to the resonance at this n in the sticking coefficient, see Fig. 11. The inset shows the full θ range.

VII. SUMMARY AND CONCLUSIONS

We have in this paper developed a theory of atom scattering off inhomogeneous Bose liquids, specifically ^{4}He, building upon ground-state methods with proven reliability and without uncontrollable modeling assumptions. Our formulation is a manifestly microscopic many-body theory, i.e., it starts from dynamic many-body wave function. The part of the formalism needed for dealing with *elastic* processes has been presented in Ref. 3. We have here introduced the concept of particle currents which are second order in the correlation fluctuations, or *transport* currents, which are necessary for the extension of the techniques of Ref. 3 to inelastic processes. We anticipate that this concept will turn out to be a useful one for many other future microscopic studies of the dynamics of many-particle systems.

Although our theory is based on a many-body wave function, we have ultimately arrived at a formulation in familiar terms like effective interactions and complex self-energies ("optical potentials"). This is expected: microscopic many-body theory simply provides a means for calculating such quantities from an underlying microscopic Hamiltonian and relates them to other observables. In our case, the theory provided information on the interaction between the helium film and its excitations and the impinging hydrogen and ^{3}He atoms.

We have then applied the theory to describe static and dynamic properties of hydrogen and ^{3}He atoms interacting with adsorbed helium films. The ground-state calculations have followed the pattern defined in Ref. 1; we expect that the present results have an accuracy of the same high quality. Our results for hydrogen supersede those of Ref. 27, which had been obtained with a much simpler, and hence less accurate, version of the same theory.

Hydrogen atoms interacting with ^{4}He films are a relatively tame problem because the impurity hardly perturbs the surface and is, unlike ^{3}He, strongly repelled by the interior of the film. As a consequence, the elastic and inelastic reflection coefficients are mostly featureless quantities, unlike the reflection coefficients of ^{3}He atoms where the coupling to resonances inside the film, and to higher-lying Andreev states, could be observed.

The sticking probability s, which vanishes linearly with the perpendicular momentum of the scattering atom, depends sensitively on the van der Waals tail of the substrate potential. Typically, s becomes large whenever, as a function of the thickness of the underlying film, a bound state turns into a shallow resonance or vice versa. We found two essentially different types of resonances, near which s becomes large: (i) in addition to the Andreev state of H of binding energy 1 K at the free ^{4}He surface, for thin films the attraction of the substrate can also introduce a broad, weakly bound excited state far above the film with a binding energy of the order of millikelvin. Upon increasing the film thickness, this excited state turns into a resonance (at approximately $n=0.8$ Å^{-2} for our generic substrate with $C_3=4400$ K Å^3, and neglecting retardation), and s can become very large. To our knowledge, these weakly bound states have not been experimentally observed, whereas the enhancement of s due to low-energy resonances has been measured.[6] Scattering of atomic hydrogen or other atoms may, thus, be a sensitive method for determining the van der Waals attraction by measuring the resonance peak(s) of s, at sufficiently low energies, as a function of the thickness of an adsorbed ^{4}He film, which acts as a buffer. (ii) Due to its negative chemical potential of −2.7 K in bulk ^{4}He, ^{3}He has, in addition to the Andreev ground state on the film surface, an increasing number of bound states in the film with increasing film thickness. The creation of these bulklike states from scattering resonances can also be seen as pronounced peaks in s.

Furthermore, the low-energy resonance induced by the substrate potential, which enhances sticking at low incident energy, also enhances, for arbitrary incident energy, direct inelastic scattering into directions almost parallel to the film: e.g., $d\sigma/d\theta$ for H scattering exhibits a peak near $\theta=\pi/2$, which is most pronounced exactly at the critical film coverage, where the low-energy resonance turns into a weakly bound state.

Since the low-energy limits of the sticking and inelastic scattering probabilities are of particular interest, we have derived analytic expressions for the direct inelastic scattering probability r_{inel} at low energies E and found $r_{\text{inel}} \propto E^2$. The surprisingly small exponent results from the long range of the interaction between long-wavelength third sound modes and the scattering atom: this allows the excitation of third sound modes when the atom is still far away from the film, where the probability density is not suppressed by universal quantum reflection. The same mechanism leads to the focusing of the inelastically scattered beam in the specular direction (quasielastic scattering) in the limit of low incident energies.

Finally, for higher scattering energies, the probability $d\sigma/dk_{\perp,\text{out}}$ to inelastically scatter from the elastic channel with momentum $\hbar k_{\text{in}}$ into a channel with outgoing perpendicular momentum $\hbar k_{\perp,\text{out}}$ was found to have an oscillatory structure, which we tentatively related to an effective range

of interaction between atom and surface excitations, which is small for H due to the repulsion from the film and of the order of the film thickness for ^{3}He.

Our work is complementary to studies of universal quantum reflection of H atoms off ^{4}He surfaces:[22,32] Whereas this phenomenon is described within the theoretical framework, many-body effects have little or no influence on more elusive problems like retardation of the substrate potential. In the end, of course, many of the *quantitative* aspects of "quantum sticking" depend on the interaction of the impinging atom with the ^{4}He surface, and the calculation of this interaction is the task of many-body physics.

Our microscopic approach contains, of course, approximations concerning both technical approximations and the physical model. Concerning the physical model, the restriction to zero temperature is the most obvious one, and one of the next tasks would be to generalize our theory, along the lines of the work of Ref. 57, to finite temperature. Technically, we must again distinguish between two levels of approximations that have been made and that warrant further investigation. One is the calculation of the diagrammatic ingredients of the theory. In particular, for the derivation of some of the long-wavelength limits, we have needed the fact that the particle-hole interactions are the variational derivative of the Hartree potentials with respect to the density. This allowed us to establish connections between microscopic interactions and macroscopic quantities like the hydrodynamic speed of sound, or the coverage dependence of the impurity chemical potential. However, there is *no* finite order approximation that satisfies these properties exactly; hence, especially our low-energy results that relied on these identities bear some uncertainty. The second approximation of the physical model is that we have considered only three-phonon processes. Evidently, it is very difficult to go beyond this approximation, and we can only estimate the regime of validity of our calculations by analogy with simpler systems where better approximations are feasible.[58] From that, we would conclude that our predictions are accurate *below* the roton energy, semiquantitative around the roton energy. However, multiphonon excitations may become very important when the energy is sufficient to excite two or more rotons.

Future research is anticipated to go into several directions: The same techniques that have been applied here can be applied for the presently more active field of atom scattering from helium clusters.[59,60] The near future will see not only experiments investigating pickup processes,[61] but also differential cross sections. Furthermore, we note that the formalism can be applied without modification also to Bose systems other than helium, such as scattering at Bose-Einstein condensates of atomic gases, where three-phonon processes are essential to understand the decay of the condensate.

The study of adsorbed films can now turn to a more detailed description of a large number of hydrogen atoms and molecules as well as ^{3}He atoms physisorbed to helium films. The adatoms form a two-dimensional gas film on the three-dimensional liquid ^{4}He, but they will, at very low coverage, dimerize. As long as the ^{4}He is assumed to provide just a static confining potential, and no dynamics, we have a two-dimensional (2D) (or pseudo-2D) Bose or Fermi gas. While such an assumption can simplify a theoretical treatment enormously, we have shown in this work that it is also very limited and leaves out much interesting and important physics. At sufficiently high coverages, the second Andreev state of the ^{3}He atoms can be macroscopically populated, giving rise to interesting thermodynamic and magnetic properties[33] as well as to a new type of Landau's Fermi liquid theory.[62]

ACKNOWLEDGMENTS

This work was supported, in part, by the Austrian Science Fund under Grant No. P12832-TPH. We would like to thank M. Hayden, M. W. Reynolds, and F. Stienkemeier for stimulating our interest in this field of research.

[1] B. E. Clements, E. Krotscheck, and M. Saarela, Phys. Rev. B **55**, 5959 (1997).
[2] C. E. Campbell, E. Krotscheck, and M. Saarela, Phys. Rev. Lett. **80**, 2169 (1998).
[3] E. Krotscheck and R. Zillich, Phys. Rev. B **58**, 5707 (1998).
[4] J. Järvinen and S. A. Vasilyev, J. Phys.: Conf. Ser. **19**, 186 (2005).
[5] A. C. Maan, B. J. Verhaar, H. T. C. Stoof, and I. F. Silvera, Phys. Rev. A **48**, 3921 (1993).
[6] I. A. Yu, J. M. Doyle, J. C. Sandberg, C. L. Cesar, D. Kleppner, and T. J. Greytak, Phys. Rev. Lett. **71**, 1589 (1993).
[7] J. Ahokas, J. Järvinen, and S. A. Vasiliev, Phys. Rev. Lett. **98**, 043004 (2007).
[8] A. I. Safonov, S. A. Vasilyev, I. S. Yasnikov, I. I. Lukashevich, and S. Jaakkola, Phys. Rev. Lett. **81**, 4545 (1998).
[9] J. Järvinen, J. Ahokas, S. Jaakkola, and S. A. Vasilyev, Phys. Rev. A **72**, 052713 (2005).
[10] I. F. Silvera and J. T. M. Walraven, Phys. Rev. Lett. **44**, 164 (1980).
[11] I. F. Silvera and J. T. M. Walraven, Phys. Rev. Lett. **45**, 1268 (1980).
[12] M. E. Hayden, S. K. Lamoreaux, and R. Golub, in *Proceedings of the 24th International Conference on Low Temperature Physics*, edited by Y. Takano, S. P. Hershfield, S. O. Hill, P. J. Hirschfeld, and A. M. Goldman, AIP Conf. Proc. No. 850 (AIP, New York, 2006), p. 147.
[13] I. B. Mantz and D. O. Edwards, Phys. Rev. B **20**, 4518 (1979).
[14] I. Shinkoda and W. N. Hardy, J. Low Temp. Phys. **85**, 99 (1991).
[15] A. I. Safonov, S. A. Vasilyev, A. A. Kharitonov, S. T. Boldarev, I. I. Lukashevich, and S. Jaakkola, Phys. Rev. Lett. **86**, 3356 (2001).
[16] M. Morrow, R. Jochemsen, A. J. Berlinsky, and W. N. Hardy, Phys. Rev. Lett. **46**, 195 (1981); *ibid.* **47**, 455(E) (1981).
[17] A. P. M. Matthey, J. T. M. Walraven, and I. F. Silvera, Phys. Rev. Lett. **46**, 668 (1981).
[18] T. Arai, M. Yamane, A. Fukuda, and T. Mizusaki, J. Low Temp.

Phys. **112**, 373 (1998).
[19] M. Saarela and E. Krotscheck, J. Low Temp. Phys. **90**, 415 (1993).
[20] W. Brenig, Z. Phys. B **36**, 227 (1980).
[21] J. E. Lennard-Jones, F. R. Strachan, and A. F. Devonshire, Proc. R. Soc. London, Ser. A **156**, 6 (1936), 1/36.
[22] C. Carraro and M. W. Cole, Prog. Surf. Sci. **57**, 61 (1998), and references therein.
[23] E. Feenberg, *Theory of Quantum Fluids* (Academic, New York, 1969).
[24] B. E. Clements, J. L. Epstein, E. Krotscheck, and M. Saarela, Phys. Rev. B **48**, 7450 (1993).
[25] C. C. Chang and M. Cohen, Phys. Rev. A **8**, 1930 (1973).
[26] D. S. Zimmerman and A. J. Berlinsky, Can. J. Phys. **62**, 590 (1984).
[27] E. Krotscheck, M. Saarela, and J. L. Epstein, Phys. Rev. B **38**, 111 (1988).
[28] E. Krotscheck, G.-X. Qian, and W. Kohn, Phys. Rev. B **31**, 4245 (1985).
[29] J. J. Berkhout and J. T. M. Walraven, Phys. Rev. B **47**, 8886 (1993).
[30] J. M. Doyle, J. C. Sandberg, I. A. Yu, C. L. Cesar, D. Kleppner, and T. J. Greytak, Phys. Rev. Lett. **67**, 603 (1991).
[31] D. G. Fried, T. C. Killian, L. Willmann, D. Landhuis, S. C. Moss, D. Kleppner, and T. J. Greytak, Phys. Rev. Lett. **81**, 3811 (1998).
[32] J. Bölheim, W. Brenig, and J. Stuzki, Z. Phys. B: Condens. Matter **48**, 43 (1982).
[33] R. B. Hallock, in *Progress in Low Temperature Physics*, edited by W. P. Halperin (North-Holland, Amsterdam, 1995), Vol. XIV, Chap. 5, pp. 321–443.
[34] C. Carraro and M. W. Cole, Phys. Rev. B **45**, 12930 (1992).
[35] A. F. Andreev, Sov. Phys. JETP **23**, 939 (1966).
[36] B. E. Clements, E. Krotscheck, and M. Saarela, Z. Phys. B: Condens. Matter **94**, 115 (1994).
[37] J. Bardeen, G. Baym, and D. Pines, Phys. Rev. **156**, 207 (1967).
[38] T. W. Hijmans and G. V. Shlyapnikov, Phys. Lett. A **142**, 45 (1989).
[39] E. Tiesinga, H. T. C. Stoof, and B. J. Verhaar, Phys. Rev. B **41**, 8886 (1990).
[40] R. A. Guyer, M. D. Miller, and J. Yaple, Phys. Rev. B **25**, 4570 (1982).
[41] J. Walraven (private communication).
[42] E. Krotscheck and M. D. Miller, Phys. Rev. B **73**, 134514 (2006).
[43] R. Jochemsen, A. J. Berlinsky, and W. N. Hardy, Can. J. Phys. **62**, 751759 (1984).
[44] G. Das, A. F. Wagner, and A. C. Wahl, J. Chem. Phys. **68**, 4917 (1978).
[45] J. P. Toennies, W. Welz, and G. Wolf, Chem. Phys. Lett. **44**, 5 (1976).
[46] G. Vidali, G. Ihm, H.-Y. Kim, and M. W. Cole, Surf. Sci. Rep. **12**, 133 (1991).
[47] R. Jochemsen, M. Morrow, A. J. Berlinsky, and W. N. Hardy, Phys. Rev. Lett. **47**, 852 (1981).
[48] R. Jochemsen and A. J. Berlinsky, Can. J. Phys. **60**, 252 (1982).
[49] V. Apaja, E. Krotscheck, A. Rimnac, and R. Zillich, in *Recent Progress in Many-Body Theories*, edited by S. Hernandez and H. Cataldo (World Scientific, Singapore, 2007), p. 81.
[50] R. de Bruyn Ouboter and C. N. Yang, Physica B & C **144**, 127 (1986).
[51] D. T. Sprague, N. Alikacem, P. A. Sheldon, and R. B. Hallock, Phys. Rev. Lett. **72**, 384 (1994).
[52] J. R. Taylor, *Scattering Theory* (Wiley, New York, 1972).
[53] M. Saarela (private communication).
[54] *Surface Phonons*, edited by W. Kress and F. W. de Wette, Springer Sereis in Surface Sciences Vol. 21 (Springer, Berlin, 1990).
[55] A. S. Sanza and S. Miret-Arts, Phys. Rep. **451**, 37 (2007).
[56] C. Holmberg, P. Apell, and J. Giraldo, Phys. Scr. **33**, 173 (1986).
[57] C. E. Campbell, B. E. Clements, E. Krotscheck, and M. Saarela, Phys. Rev. B **55**, 3769 (1997).
[58] V. Apaja and M. Saarela, Phys. Rev. B **57**, 5358 (1998).
[59] E. Krotscheck and R. Zillich, J. Chem. Phys. **115**, 10161 (2001).
[60] E. Krotscheck and R. E. Zillich, Eur. Phys. J. D **43**, 113 (2007).
[61] J. Harms and J. P. Toennies, Phys. Rev. Lett. **83**, 344 (1999).
[62] R. H. Anderson and M. D. Miller, Phys. Rev. B **40**, 2109 (1989).